

Online Research @ Cardiff

This is an Open Access document downloaded from ORCA, Cardiff University's institutional repository: <https://orca.cardiff.ac.uk/id/eprint/131298/>

This is the author's version of a work that was submitted to / accepted for publication.

Citation for final published version:

Ji, Hongyu, Pan, Shunqi ORCID: <https://orcid.org/0000-0001-8252-5991> and Chen, Shenliang 2020. Impact of river discharge on hydrodynamics and sedimentary processes at Yellow River Delta. Marine Geology 425 , 106210. 10.1016/j.margeo.2020.106210 file

Publishers page: <http://dx.doi.org/10.1016/j.margeo.2020.106210>
<<http://dx.doi.org/10.1016/j.margeo.2020.106210>>

Please note:

Changes made as a result of publishing processes such as copy-editing, formatting and page numbers may not be reflected in this version. For the definitive version of this publication, please refer to the published source. You are advised to consult the publisher's version if you wish to cite this paper.

This version is being made available in accordance with publisher policies.

See

<http://orca.cf.ac.uk/policies.html> for usage policies. Copyright and moral rights for publications made available in ORCA are retained by the copyright holders.



Highlights

- (1) Tide amplitude decreases in the lowermost channel and tidal flats of the Yellow River Delta as river discharge increases.
- (2) The river discharge changes can reshape the shear front zone dynamics near the active Yellow River delta.
- (3) The barrier effect of the tidal shear front zone combined with strong longshore tidal currents significantly restrict the sediment dispersal and river mouth deposits.

Impact of river discharge on hydrodynamics and sedimentary processes at Yellow River Delta

Hongyu Ji ^{a,b}, Shunqi Pan ^{a,b}, Shenliang Chen ^{a*}

^a State Key Laboratory of Estuarine and Coastal Research, East China Normal University,
Shanghai 200241, China.

^b Hydro-environmental Research Centre, School of Engineering, Cardiff University, Cardiff
CF24 3AA, UK.

* Corresponding author.

Tel: +86 (0)21-54836498

Email Address: slchen@sklec.ecnu.cn (S. L. Chen)

Highlights

(1) Tide amplitude decreases in the lowermost channel and tidal flats of the Yellow River Delta
as river discharge increases.

(2) The river discharge changes can reshape the shear front zone dynamics near the active
Yellow River delta.

(3) The barrier effect of the tidal shear front zone combined with strong longshore tidal currents
significantly restrict the sediment dispersal and river mouth deposits.

Keywords

Tidal dynamics; River discharge; Tidal shear front; Suspended sediment transport; Active
Yellow River Delta

Abstract

During the Anthropocene, regulating river discharge by high dams may have met the need for water demands in river basins, but resulted in carrying less freshwater and sediment to the sea, inducing land degradation and shoreline retreat in worldwide mega-river deltas. In land-ocean interaction, tide response to water discharge changes plays an important role and is crucial for the river-laden sediment transfer and dispersal, affecting both nearshore and estuarine deposits. The Yellow River Delta (YRD), which is under an increasing pressure of the new discharge regime of the Yellow River, has undergone drastic changes in terms of sediment dynamics and morphologic evolution. To gain a better understanding of the overall fluvial and marine hydrodynamics and morphodynamic processes in the YRD, in this study, a full-scale numerical model is built to investigate the interaction and impacts of changing environmental forcing and dynamics on flow and sediment transport in the estuary of YRD and its adjacent coasts. The results show that the river discharge strongly affects the tidal dynamics and morphology of the delta, particularly in the close vicinity of the outlet and the intertidal zone. Tidal constituents M2 and K1, which are the most significant ones in the YRD, are found to be noticeably affected with a decreasing trend when the river discharge increases. The model results also indicate that river discharge affects the location and intensity of the shear front that occurs in the nearshore areas of the YRD. Increasing the river discharge can induce a seaward movement of the shear front, reduce its width and concentrate its shear intensity. It is found that the reverse of the flow direction at each side of the shear front and strong longshore tidal current can act as a barrier for the sediment dispersal process by keeping suspended sediment in the inner zone, thus to form a particular sediment deposition zone and the depo-center.

1. Introduction

Sustainability of river deltas becomes one of the major challenges in this century. Natural processes and intensified human activities are shifting the balance between the river and coastal ocean dynamics, inducing changes in coastal and estuarine environments (Syvitski and Saito, 2007; Nienhuis et al., 2018). Due to the integrated effects of sediment starvation, land reclamation and relative sea level rise, river deltas tend to be more easily exposed to marine processes (Hoitink et al., 2017), led to a trend of land loss and shoreline retreat (Blum and Roberts, 2009). With the growing concerns about the morphologic adjustments to the changing coastal environment globally (Dai et al., 2014; Luan et al., 2016; Jiang et al., 2018; Maloney et al., 2018), studying the patterns and rates of delta growth becomes essential for understanding the effects of human perturbations on river deltas with rapid environmental changes (Chamberlain et al., 2018).

Interaction between the river discharge and nearshore tides can play a key role in the morphodynamic development of deltas (Hoitink et al., 2017), as it acts as an important factor in controlling both river mouth hydrodynamics and estuarine deposits (Leonardi et al., 2013; Leonardi et al., 2015). For example, Leonardi et al. (2013) focused on the role of tides in shaping river mouth bar morphology in the fluvial dominated case and tidal dominated case, respectively, while Leonardi et al., (2015) suggested by field observations that even in micro-tidal environments, tides can play a critical role in shaping distributary hydrodynamics during both low and high river discharge regime. As indicated by Cai et al. (2014), the increase of riverine runoff can promote tidal damping, and reduce tidal velocity amplitude and wave celerity in the upstream channel of the estuary, but to what extent the riverine runoff variations will influence on the tidal dynamics in the coastal area near the river mouth still remains unclear and deserves further investigations.

The Yellow River Delta (YRD), which is located in the northern coast of China adjacent to the Bohai Sea and one of the largest deltas in the world, has undergone drastic changes in hydrodynamics and morphodynamics. Recent studies showed that the land reclamation, sea level rise and rapid submarine topographic changes may have affected the dominance of the regional fluvial and coastal dynamics in the Bohai Sea (Pelling et al., 2013). Specifically, Huang et al. (2015) and Zhu et al. (2018) analysed the impacts of the coastline modifications and reclamation projects on the evolution of the tidal system in the Bohai Sea, and found the amphidromic point near the YRD having moved south-eastwards gradually. Li et al. (2016) investigated the potential effect of sea level rise on the tidal dynamics of the Bohai Sea. However, little attention has been paid to the changing environment on the variation of tides near the YRD, especially with the decreasing trend of river discharge.

Where there is a strong interaction between the fluvial discharge and coastal tides, an estuarine shear front can be formed. This marine front in general occurs along the shearing interface between two fluid bodies of the tide flow with reverse flow directions (Li et al., 2001). In this transition zone, large gradients of flow velocity, suspended sediment concentration (SSC), salinity and temperature can often be found (Wang et al., 2007). The dynamics and movement of the shear front have critical effects on the suspended sediment transport and dispersal patterns in the estuaries and coastal zones (Huzzey and Brubaker, 1998; Nunes and Simpson, 1985). For the YRD, the extremely high sediment deposition rate can certainly be associated with the high sediment discharge from the river, and enhanced from the barrier effect from the shear front (Wang et al., 2007; Zhou et al., 2015; Wang et al., 2017a). The latter largely restricts the fine suspended sediment dispersal, and it is found that about 68% of the fine suspended sediment is deposited near the active YRD (Ji et al., 2018). Field observations (Li et al., 1998, 2001; Wang et al., 2007; Bi et al., 2010; Yang et al., 2011; Wu et al., 2015) and numerical studies (Qiao et al., 2008; Wang et al., 2017a) have well illustrated that the formation and

spatial-temporal dynamics of the shear front in the YRD is the main cause for the large sloping nearshore morphology and its changes. Although the long-term evolution of the shear front in the YRD was investigated (Wang et al., 2017a), its local dynamics in the active YRD is still unclear, especially under the present landscape and new regime of river input.

Over the recent decades, under the influence of both the human interventions and climate change in the river basin, the YRD receives a drastically decreased river input, but with a highly inter-annual variability (Liu et al., 2012), mainly due to the Water-Sediment Regulation Scheme (WSRS) in the upstream of the low reach of the Yellow River controlled the dam at Xiaolangdi. The WSRS can result in approximately 30% and 50% of annual water and sediment discharges being transported to the sea respectively over a short period (Yu et al., 2013), which is much larger than the river discharge during natural flood seasons. A number of studies have been carried out focusing on the potential effect of the new river discharge regime on the enhanced spread of nutrients (Wang et al., 2017b), shoreline dynamics (Fan et al., 2018a), morphological changes in subaerial delta (Bi et al., 2014) and subaqueous delta (Ji et al., 2018). However, little has been done regarding influence of the inter-annual variability of the river input on the tidal dynamics, sediment dispersal range and sedimentation processes. The sediment dynamics influenced by the interactions between the river and coastal ocean can also have potential modifications to the deltaic depo-center, which is crucial to the land-building against the sea level rise due to the climate change.

Therefore, in this study, a 2D depth-averaged numerical model based on TELEMAC suite (Hervouet, 2007) is established and applied to simulate the tidal and sediment dynamics in response to the variations of river input. This work, for the first time, is to focus on the effect of river flow on the location and dynamics of tidal shear front and its influence on the sedimentary processes. The specific objectives of this study are: (1) to investigate the tide amplitude variations of the receiving basin to the river discharge changes; (2) to identify the

tidal shear front dynamic response to the river input and consequent impacts on flow velocity and SSC changes across the shear front; and (3) to study the influence of the shear front dynamics to the deposits around the river mouth.

2. Study Area

The Yellow River originates from Qinghai-Tibet Plateau and flows through the Loess Plateau and North China Plain successively, finally empties into the Bohai Sea (Figure 1a). With high flow and highly concentrated sediment discharge deliveries, rapid deposition and frequent channel avulsions have occurred in the YRD over recent decades, forming a fan-shaped landscape. The active deltaic lowermost channel has migrated from Shenxiangou (SXG) channel (1953-1964) and Diaokouhe (DKH) channel (1964-1976) to the current Qingshuigou (QSG) channel (1976-present), during which an artificial diversion to a new mouth channel known as Q8 channel (Chu et al., 2006) became necessary due to the concerns of the stability of QSG channel and decrease in the potential risk of flooding (Peng et al., 2010), as shown in Figure 1b. The orientation of the active mouth channel has changed from the east direction to the north in 2007, and bifurcated into the North River mouth (NRM) and the East River mouth (ERM) since 2013.

However, due to the changing natural environment (temperature and precipitation) and river damming in the upstream (Figure 1a), the riverine deliveries of both water and sediment have been seen a dramatic decrease (Jiang et al., 2017). The mean water discharge since 2000 only reached 749 m³/s in the flood seasons, being about 31% of 1950-1985 level (Figure 2a). For the purpose of flooding prevention and agricultural use, the water discharge is highly regulated and distributed throughout the year (Wang et al., 2006a), except for the human-induced peak-flood during WSRS. The sediment discharge has also dramatically decreased from 10.5×10⁸ t/yr in 1950-1985 to 1.13×10⁸ t/yr in 2000-2017 (Figure 2b), with a drastic decline of the SSC

from an average level of 29.0 kg/m³ before 2000 to 6.6 kg/m³ after 2000 (Figure 2c). The sediment grain size recorded at Lijin Station shows an increasing trend after the implementation of WSRS, as the heavy sedimentation behind the dams and in the lower reach (Figure 2d), which results sediment coarsening in recent years.

As regards the tidal regime off the YRD, it has been well accepted that it is dominated by an irregular semi-diurnal tide with a mean range of 0.73-1.77 m (Yang et al., 2011). Tides and tidal currents are highly influenced by the amphidromic point of tidal constituent M2 located offshore in Shenxiangou channel (Fan and Huang, 2005). Tidal current is found to be generally parallel to the coastline, which flows southward during flood tide and northward during ebb tide with an average speed of 0.5-1.0 m/s (Bi et al., 2010).

3. Methodology

3.1 Model set-up

A 2D depth-averaged coupled hydrodynamic and morphodynamic model based on the open-source TELEMAC suite (Hervouet, 2007) is set up for this study. The computational domain, centred at the YRD, spans from 37 to 41°N in latitude and from 117.5 to 122°E in longitude, covering the entire Bohai Sea and part of Yellow Sea, as shown in Figure 3. The model uses an irregular (triangular) mesh with 168938 nodes, 335171 elements and varying grid resolution from 8 km near the open boundary to around 50 m in the river channel and the estuary.

The hydrodynamic module in the model TELEMAC2D solves the following 2D depth-averaged Navier-Stokes equations:

$$\frac{\partial h}{\partial t} + \vec{u} \cdot \vec{\nabla}(h) + h \operatorname{div}(\vec{u}) = S_h \quad [1]$$

$$\frac{\partial u}{\partial t} + \vec{u} \cdot \vec{\nabla}(u) = -g \frac{\partial z}{\partial x} + S_x + \frac{1}{h} \operatorname{div}(h \nu_t \vec{\nabla} u) \quad [2]$$

$$\frac{\partial v}{\partial t} + \vec{u} \cdot \vec{\nabla}(v) = -g \frac{\partial z}{\partial y} + S_y + \frac{1}{h} \text{div}(h v_t \vec{\nabla} v) \quad [3]$$

where, u & v are the depth-averaged velocity in x and y direction, h is the water depth, v_t is the momentum diffusion coefficient, and S_x and S_y are the source or sink terms within the domain.

The sediment transport module SISYPHE is coupled with the hydrodynamic module for computing sediment transport and bed level changes. In this study, due to the fact that the morphodynamic process is dominated by the fine sediment, only the suspended sediment transport is considered by solving the two-dimensional advection-diffusion equation, expressed as:

$$\frac{\partial hC}{\partial t} + \frac{\partial huC}{\partial x} + \frac{\partial hvC}{\partial y} = \frac{\partial}{\partial x} (h \varepsilon_s \frac{\partial C}{\partial x}) + \frac{\partial}{\partial y} (h \varepsilon_s \frac{\partial C}{\partial y}) + \alpha \omega (S_* - S) \quad [4]$$

where, $C=C(x,y,t)$ is the depth-averaged concentration expressed in volume concentration, ε_s is the turbulent diffusivity of the sediment, S is the near-bed concentration, S_* is the sediment transport capacity under tidal currents, and ω is settling velocity, which can be calculated with the following expression for the sediment grain diameter d_{50} less than 100 μm :

$$\omega = \frac{(s-1)g d_{50}^2}{18\nu} \quad [5]$$

where ν is the kinematic viscosity.

Given the particular characteristics of the fine sediment transported in the Yellow River, it is necessary to implement a user-defined function in the model to calculate the sediment transport capacity (S_*) with the formula proposed by [Dou et al. \(1995\)](#):

$$S_* = \alpha_0 \frac{1}{\omega(s-1)} \frac{r^3 n^2}{h^{4/3}} \quad [6]$$

where, r is the resultant velocity of u & v , n is Manning's coefficient for bed roughness, s is the specific density of sediment to water, and α_0 is a constant (0.023).

For bed evolution when only the suspended sediment is considered, the following formula is used:

$$(1 - \lambda) \frac{\partial Z_b}{\partial t} = \alpha \omega (S - S_*) \quad [7]$$

where, λ is the bed porosity and Z_b is the bed level.

In this study, the topography data is taken from two sources: the bathymetric survey carried out in 2015 for the YRD lowermost channel and the subaqueous delta, and the bathymetric survey carried out in 1999 for other subaqueous areas in the Bohai Sea. The seaward open boundary located in the northern Yellow Sea is driven by the tidal elevations and depth-averaged velocity from TPXO7.2 database (<http://volkov.oce.orst.edu/tides>) with 13 tide constituents, namely M2, S2, N2, K2, K1, O1, P1, Q1, MF, MM, M4, MS4 and MN4. The upstream boundary is located at the transect of the lowermost channel of the YRD, some 40 km from the estuary mouth, where representative flow discharge is imposed to represent the river discharge at the most downstream hydrograph station, Lijin Station, as shown in Figure 3.

3.2 Model validations

The model performance is assessed by evaluating the root-mean-square error (RMSE) and the correlation efficient (CC) between the computed results and observations with the following expressions:

$$RMSE = \sqrt{\frac{\sum (X_{cal} - X_{obs})^2}{N}} \quad [8]$$

$$CC = \frac{\sum (X_{cal} - \bar{X}_{cal})(X_{obs} - \bar{X}_{obs})}{[\sum (X_{cal} - \bar{X}_{cal})^2 \sum (X_{obs} - \bar{X}_{obs})^2]^{1/2}} \quad [9]$$

where, X_{cal} and X_{obs} are the values of model calculated and observed qualities, respectively. N is the numbers of X_{obs} , and \bar{X}_{cal} and \bar{X}_{obs} are the time average values of X_{cal} and X_{obs} , respectively.

During the validating, the model is operated with a constant river discharge 500 m³/s at upstream boundary for two periods: from 1 June 2015 to 15 June 2015 and from 25 August 2018 to 31 August 2018. The former is used to validate the water levels and the latter is used to validate the flow velocities and directions near the YRD.

Figure 4 shows the water level comparisons between model computed results and tide gauge data. The RMSE values for the water levels at twelve tidal gauge stations along the coast of the Bohai Sea range from 8.2 to 28.2 cm, with an average standard deviation of 16.1 cm. The CC values between model results and observations all reach 0.84, except for QHD and DYG Stations, where the tides are likely to be complicated by the nearby amphidromic points.

Figure 5 shows the comparisons of the velocity magnitude and flow directions between in-situ observations and model computations near Diaokouhe abandoned estuary (O1 and O2), Gudong littoral zone (O3 and O4) and the active YRD (O5 and O6). The depth-averaged velocity was calculated by the velocities observed at different layers by acoustic Doppler current profilers (ADCPs). It can be seen that the depth-averaged flow direction agrees well with the observations. The RMSE values at six observation points range from 5.6-30.2 cm/s, with CC values reaching 0.80 except for that at O2. In general, the model validation indicates that the model performs well overall in the tide dynamics.

Due to the lack of field observations of SSC in the study area, the computed SSC from the model is then compared with the remote sensing image of calm weather. A remote sensing image in Oct. 2014 with light wind is chosen to represent the sediment dispersal near the river mouth. The simulated surface wind from the European Centre for Medium-Range Weather

Forecasts (ECMWF) (<http://apps.ecmwf.int/datasets/>) shows the wind velocity was 2.0-5.0 m/s in latitude direction and 0.1-0.4 m/s in longitude direction, when the effect of wind waves on sediment resuspension was assumed to be neglectable. The results show that two high-turbidity areas located at the north (Diaokouhe) YRD and the active YRD both in the remote sensing image and computed results (Figure 6). The high current velocity in both sites is considered to be the key driving factor for sediment resuspension and transport processes, forming high turbidity zones (Fan et al., 2018b). Wind waves and storm surges can promote this process. Even though wave conditions are not considered in the model, the spatial distribution of SSC is largely consistent with that in Landsat 8 image in fair weather (Figure 6) and the distributions of suspended particulate matter estimated by Qiu et al. (2017), which proves that our sediment module can reflect the sediment dynamics in the YRD.

4. Results and Discussion

4.1 Model conditions

The validated model is then applied to examine the effect of the river discharge on tides in both far-field and near-field and to investigate the impacts on the shear front. The model is run with 2 cases. In Case 1, which is focused on the hydrodynamics, the model is run with 5 representative flow discharges: 0 m³/s, 500 m³/s, 1000 m³/s, 4000 m³/s and 10000 m³/s, without considering sediment transport (i.e. hydrodynamics only). Amongst the no-flow case (0 m³/s) is used as the reference case, while 500 m³/s represents the average river discharge in dry seasons, 1000 m³/s represents the average river discharge in flood seasons and 4000 m³/s is the average peak flood discharge during WSRS. River flow of 10000 m³/s is also regarded as the design extreme discharge for the current flood defence in the YRD. In Case 2, which is focused to capture the effect of river discharge on the dynamics of the shear front and sedimentation processes, the model is driven by 3 different discharges, namely 500 m³/s (low water discharge),

2000 m³/s (middle water discharge) and 3000 m³/s (high water discharge). At the upstream river boundary, equilibrium concentrations of sediment is assumed. As shown in [Figure 2d](#), the median grain size from long-term time series analysis at Lijin Station was in a range between 16.4 µm and 23.0 µm. The field observation in 2013 also showed a great spatial variability in the YRD, ranging from 6.3 µm to 119 µm. By considering the complex pattern of sediment size in the study area, it is decided that a median grain size of 16 µm (fine silt) is chosen to represent the influx sediment at the active river mouth.

4.2 Tidal response to the changing environment

4.2.1 Tide dynamics in the Bohai Sea

In Case 1, the model is run for a period of 45 days with a series of prescribed river discharges. Tide harmonic analysis is carried out using T_Tide codes ([Pawlowicz et al., 2002](#)) on the computed water levels for the latter 30 days to eliminate the initial effect in the first 15-day lead-in period. For the period of 30 days, which covers just over 2 spring-neap tide cycles, the hourly output of the model results is believed to be sufficient for analysing the main tide constituents. Tide amplitude and phases for M2, S2, O1 and K1 tidal constituents are presented in [Figure 7\(a-d\)](#). The results are in general agree with the observations and model simulations from other researchers ([Huang et al., 2015](#); [Zhu et al., 2018](#)). Two amphidromic points of M2 and S2 in the Bohai Sea: one is located at QHD and the other is close to the northern part of Gudong. The computed results show that with the nearshore topography changes of the YRD and coastline variations in the Bohai Sea, the M2 amphidromic point found in this study have moved slightly southwards from the coast off the Wuhaozhuang to the north of Gudong in recent years, which is in well agreement with the result from [Huang et al. \(2015\)](#).

[Figure 7e](#) shows distribution of total tide ranges in the Bohai Sea. It can be seen that the central area in the Bohai Sea is dominated by micro-tides with the tide range being less than 2 m. The areas in the east, north and west of the Bohai Sea are of meso-tides with tide range being

between 2 and 4 m. In the far north end of the Bohai Sea, it is the region of macro-tides where the tide range exceeds 4 m.

As for the type of the tides in the Bohai Sea, the classification suggested by [Reeve et al. \(2004\)](#) is used. The type of tides in the region is determined with the following expression:

$$F = \frac{K1+O1}{M2+S2} \quad [10]$$

where M2, S2, O1 and K1 are the amplitudes of respective tidal constituents. From Eq. 10, when $F < 0.25$, the tides can be classified as the semidiurnal type and while $F > 3.0$, the tides are of the diurnal form. When F is between 0.25 and 3.0, the tides are of the mixed type. In the Bohai Sea, most of the area is dominated with mixed tides, where tides around two amphidromic points are diurnal, and areas in the southeast Bohai Sea are semidiurnal as shown in [Figure 7f](#). The results also indicate the YRD coastal regions mainly belong to microtidal category near the Yellow River mouth, and the tidal range gradually increases westward and southward, belonging to meso-tides in the west of Diaokouhe estuary and Laizhou Bay on south of the YRD. Furthermore, near the M2 and S2 amphidromic points in the north of Gudong, the tides are of the diurnal tide type, and gradually vary to the mixed type to the other vicinity of the YRD.

4.2.2 Effect of river discharge on coastal tides of the YRD

As indicated in [Figure 7](#), M2 and K1 are the largest tidal amplitudes, thus the most significant tidal constituents in the Bohai Sea. Therefore, tidal amplitudes of M2 and K1 near the YRD coast are computed with the prescribed river discharges and compared with the reference case of no river discharge condition, and their differences are shown in [Figure 8](#). It can be seen that when the river discharge increases, the tidal amplitudes of both M2 and K1 show a remarkable decreasing trend in the lowermost channel of the YRD within the iso-depth of 0 m. With a lower river discharge, the tidal waves can propagate further into the channel and the flow

direction in the estuary is bidirectional. But with the increased river discharge, the tidal waves can be blocked further seaward and the tidal amplitudes can be depressed by the river discharge as shown in Figure 8. For M2 tides, the reduction of the tidal amplitude is found in a range between 0.02 m with river discharge of 500 m³/s and 0.1 m with river discharge of 10000 m³/s (Figures 8a-d). A similar range can also be found for K1 tides (Figures 8e-h).

In addition, the impact of river discharge to the amplitude of M2 and K1 shows a gradually decreasing trend when coming to the margin of the river mouth. And when it comes to the vicinity out of the river mouth, the influence can be limited within 0 to -0.01 m, which is much less than that at the river mouth. When the river flow rate gradually increases, eventually the flow direction near the river mouth is believed to become unidirectional (Leonardi et al., 2013), and the tidal impact will be almost ignored regarding of fluvial processes from the upstream.

For the temporal variations of the water level, the model results are extracted at an inter-tidal location P0 as an example, as shown in Figure 9. The result indicates that the low water levels at P0 increases with the increase of the river discharge from 0 to 10000 m³/s, both during spring and neap tides, whilst the tidal range at P0 shows a drastic decreasing trend when the river discharge increases.

4.3 Dynamic response of the shear front to the river discharge

As shown in Figure 1b, the active YRD is bifurcated by the NRM distributary and the ERM distributary, which respectively has distinctive river-tides interaction processes because of the river discharge and morphological difference between them. To further investigate the dynamics response of the shear front to the river flow discharge and its difference at two bifurcated river mouth, three further simulations with different river discharges are carried out in Case 2, with a focus on morphodynamics. Given the fine sediment at the active YRD, the model simulations only consider the suspended sediment transport with the equilibrium

concentration as the upstream river boundary condition. To account for the dynamic nature of the shear front, fully developed shear fronts of both front types are selected for spatial analysis.

4.3.1 Formation and characteristics of the shear front

The tidal shear front is a shear interface with significant gradients in flow velocity, sediment concentration, temperature and salinity, which is closely attributed to the local tidal dynamics and related to the local dynamic environment and estuarine morphological changes (Wang et al., 2006b). In the YRD, the formation of shear front is associated with the phase lag between the near-field and far-field tides. The flow direction inside and outside the tidal shear front is reversed and can be categorized as IFOE (inner-flood-outer-ebb) and IEOF (inner-ebb-outer-flood) types. In this study, the location of the shear front zone is represented with its centreline, as shown in Figure 10, determined from an obvious interface where relatively low flow velocity (less than 0.1 m/s in this study) occurs compared with the velocities on both sides of the shear front.

To further analyse the formation and propagating process of the shear front near the YRD, the hourly dynamics of the shear front over a tidal cycle is extracted, as shown in Figure 11. During a tidal cycle, an IFOE type and IEOF type appear successively near the YRD. As for the IFOE type shown in Figure 11a, the shear front originates from the northern coast outside Wuhaozhuang as indicated by line 1 and propagates gradually from the northern YRD to the south (indicated by line 2 & 3). Meanwhile, at the active YRD, a sub-shear front can also be found to originate close to the shoreline as indicated by line1' and gradually move seaward to merge with line 2. The propagation process of the IEOF type is similar to the IFOE type from the north to south and from nearshore to offshore, as indicated by lines 4 (or 4') to 7 in Figure 11b. Each type of shear front lasts 3-4 hours over a tidal cycle, which generally agrees with the results of Wang et al. (2017a).

In addition, the duration of the occurrence of the shear front may play an important role in the sediment transport processes. Taking two reference points P1 and P2 as shown in [Figures 11](#), which are located at each side of the shear front with the water depth of 2 m and 16 m respectively for further analysis. [Figure 12](#) illustrates the flow directions at these 2 points over 2 tide cycles. The duration of the occurrence of the shear front in the active YRD can be derived from the phase difference of the flows. The results show that the duration for the IEOF type of the shear front is much longer than that of the IFOE type, which can act as the lateral blockage to the cross-shore transport processes, including the suspended sediment as suggested by [Wang et al. \(2007\)](#).

4.3.2 Dynamics response of the shear front to the river discharge change

[Figure 13](#) shows the dynamics of the shear front with different fluvial discharges. The results reveal that with the increase of the fluvial discharge, the shear front near the NRM remains almost the same, but the shear front at the ERM has a noticeable seaward movement. This reveals that the tide dynamics is more active and related to the fluvial dynamics from the river discharge near the ERM, in contrary to the relatively stable tide dynamics near the NRM. The field observations also indicated that the ERM distributary has gradually been the main distributary to accommodate the river discharge in respect to the NRM distributary ([Chen et al., 2019](#)). As the mean water depth at the ERM distributary is about 5 m, much shallower than the water depth at the NRM distributary (about 10 m), this may make the shear front in the ERM distributary more sensitive to the river runoff. Therefore, it can be expected that when an extreme river discharge occurs in the Yellow River either naturally or artificially, the hydrodynamics of the ERM distributary can be significantly influenced. It can also be seen that the width of the shear front zone decreases both in IFOE and IEOF front with river discharge increases ([Figure 13](#)), where the shear intensity can be concentrated with the increasing river discharge, which could impact on the sediment deposition in this area.

To investigate the hydrodynamics response to the river discharge changes at the inner and the outer areas of the shear front, two cross-sections at the NRM and ERM distributary are selected as indicated as S1 and S2 in Figure 13. These two sections are particularly selected to ensure their orientations to be nearly perpendicular to the nearshore tidal currents. Flow velocities perpendicular to the sections with 50 m resolution are extracted when the shear fronts are formed, as shown in Figure 14. It is clear that for the IFOE shear front, the inner velocities are southerly, and the outer velocities are northerly along both S1 and S2. The reversal velocity patterns can be found for the IEOF shear front. It can be also seen that the velocities on the inner side of the shear front can generally become stronger with the increase of the river flow discharge, whilst the velocities on the outer side have a quite limited response.

As also shown in Figure 14, the locations of the crossing points where the velocity magnitude is zero for different river discharges vary. The crossing point moves seaward when the river discharge increase for both types. However, the maximum difference along S1 is approximately 200 m, whilst that along the S2 is approximately 500 m. This also echoes the strong dynamic response of the shear front to the river discharge in the ERM distributary as shown in Figure 13.

4.3.3 Implications for suspended sediment transport and sedimentation

In Case 2, the model is run with the sediment transport module SISYPHE coupled. Similar to Figures 14, Figures 15 shows the SSC distributions along S1 and S2. The results show that the SSC distributions near the fully-developed shear front exhibit different patterns from the velocity distributions. Along S1, the SSC decreases drastically from the inner to the outer shear front zone with different river discharge and the SSC of the outer shear front zone is found to be limited (Figures 15a&b), which indicates the shear front at the active YRD has a potential effect on the suspended sediment dispersal to the outer sea. Along S2, where the main distributary locates to receive the water and sediment loads from the river, the SSC is higher in

comparison with that along S1 for the NRM distributary, following a general decreasing trend from the inside to the outside of the shear front (Figures 15c&d). It should be noted that the SSC distribution at the outer shear front zone of the ERM is increasing respect to the SSC at the shear front zone (Figure 15d). Because when the riverine discharge is high enough, it could break through the barrier effect of the tidal shear front at a local scale, may transport substantial riverine sediment to the out sea off the shear front, which is also proved in Figure 13.

Previous studies have demonstrated the hypopycnal flow as a main sediment transport mechanism in flood seasons of the 1980s and 1990s, and replaced by buoyant hypopycnal plume under low SSC deliveries (Wright et al., 1986, 1988, 1990; Wiseman et al., 1986; Wang et al., 2010; Yu et al., 2013). The formation of the tidal shear front at the active YRD could very likely have a potential barrier effect on the sediment dispersal to the sea. To further investigate sediment transport pathways at times without the appearance of the shear front, the suspended sediment dispersal processes during the maximum flood and ebb velocity phases are presented in Figure 16a&b. The model results show that the river-laden sediment debouching to the two mouth outlets can only be transported within a restricted area, most of which is dispersed within 10 m depth. Due to the strong coast-parallel tidal currents, even with the absence of the shear front, sediment is founded to be transported in alongshore direction, southward during the flood phase in the tide cycle and northward during ebb phase. In addition, the water depth in the Qingshuigou mouth and northern abandoned Diaokouhe estuary is relatively shallow, which, together with high velocity during the maximum flood and ebb, could trigger sediment resuspension, as indicated by two high turbid zones in the Qingshuigou Delta and the north abandoned Diaokouhe Delta in Figure 16a. For the morphological changes over 30-day simulation period, the depo-center is found to have an over 1 m deposition depth, located within 2-3 m isobaths around the outlet of the ERM for the case with low water discharge (Figure 16c), because the ERM distributary is the main distributary for the river

discharge. When the river discharge increases, the depo-center moves seaward within 3-8 m isobaths and reaches a maximum of 4 m deposition depth (Figure 16d). This is because that under the high river discharge, the shear front moves seaward and the river-laden sediment tends to be transported to a larger spatial range, further from the shore. This finding agrees with the results of Wang et al. (2007), showing that at the old Qingshuigou River mouth, the estuarine deposits are almost found within the shear front. The location of the depo-center from this study confirms that from Jiang et al. (2017), with the field observations indicating that the main underwater sedimentary body can be strongly shaped by the irregular ellipses with the long axis parallel to the 5-10 m isobaths and short axis perpendicular to the isobaths in long-term YRD morphologic evolution.

The previous studies, which mostly were focused on the effect of riverine flow and sediment delivery to the delta-building, significantly advanced the understanding of the complex processes of rapid development of the subaerial land and sedimentation in the subaqueous slope in the basin of the YRD, which receives an average of 1.08 billion tons of sediment (Milliman and Meade, 1983). However, under the changing environment, such as sea level rise, increase of storminess, intensified human activities and decrease of river input, the river-dominated YRD is also undergoing a transformation in morphodynamics. The role of tides interacting with river input is playing a more critical role in shaping the deltaic depositional system. This study uses an advanced numerical modelling framework to improve the understanding of the river discharge forcing on tidal dynamics and sediment transport in the YRD and adjacent coasts by fully considering their interaction. Under the new regime of river input, it is of profound importance to pay attention to the changes in the interactions between the river and marine processes in the estuarine depositional system.

5 Conclusions

A full-scale hydrodynamic and sediment model using the latest detailed bathymetric data of the YRD has been built to investigate flow and sedimentary processes under the changing environment. The extent of influences of the river discharge to the tidal dynamics of the YRD is fully analysed, including tidal amplitude and tidal shear front dynamics, which can have significant impact on the suspended sediment transport and deposits. The results show that, with the increases of river discharge, the amplitude of M2 and K1 tidal constituents both show a remarkable decreasing trend, both in the YRD lowermost channel and the tidal flats. In addition, the model result proves the tidal shear front propagates from the north to the south and from nearshore to offshore, lasting 3-4 hours during a tidal cycle, dominating the active YRD with IEOF type of the shear front. With river discharge increases, the shear front zone near the active YRD is forced to move seaward with the decrease in width and concentrate in the shear intensity, which becomes more obvious in the ERM from the NRM. Due to the barrier effect of the shear front and strong longshore tidal currents, the river-laden sediment can only transport within 10 m depth, forming the depo-center at the river mouth outlet. Consequently, the depo-center tends to move seaward when the river discharge increases, as the river-laden sediment disperses to a larger range with the movement of the shear front zone.

Acknowledgements

This study was partly supported by the National Key Research and Development Program of China (No.2017YFC0405503), the National Science Foundation of China (NSFC, No.U1706214), the Open Research Fund of SKLEC (SKLEC-PGKF201903), and the joint PhD programme of the China Scholarship Council for Overseas Studies (No. 201806140079). We would also like to acknowledge the Yellow River Conservancy Commission, Ministry of

Water Resources of China for providing the hydrographic data, and the European Centre for Medium-Range Weather Forecasts for providing the surface wind data.

References

Bi, N., Yang, Z., Wang, H., Hu, B., Ji, Y., 2010. Sediment dispersion patterns off the present Huanghe (Yellow River) subdelta and its dynamic mechanism during normal river discharge period. *Estuarine, Coastal and Shelf Science*, 86, 352-362.

Bi, N., Wang, H., Yang, Z., 2014. Recent changes in the erosion–accretion patterns of the active Huanghe (Yellow River) delta lobe caused by human activities. *Continental Shelf Research*, 90, 70-78.

Blum, M.D., Roberts, H.H., 2009. Drowning of the Mississippi Delta due to insufficient sediment supply and global sea-level rise. *Nature Geoscience*, 2(7), 488-491.

Chamberlain, E.L., Törnqvist, T.E., Shen, Z., Mauz, B., Wallinga, J., 2018. Anatomy of Mississippi Delta growth and its implications for coastal restoration. *Science Advances*, 4, eaar4740.

Cai, H., Savenije, H.H.G., Jiang, C., 2014. Analytical approach for predicting fresh water discharge in an estuary based on tidal water level observations. *Hydrology and Earth System Sciences*, 18 (10), 4153-4168.

Chen, S., Xu, C., Yu, S., Fan, Y., Gu, G., 2019. Water and sediment dynamics of the active Yellow River mouth and its evolution of distributary channels. *Yellow River*. (Accepted, in Chinese with English abstract)

Chu, Z.X., Sun, X.G., Zhai, S.K., Xu, K.H., 2006. Changing pattern of accretion/erosion of the modern Yellow River (Huanghe) subaerial delta, China: Based on remote sensing images. *Marine Geology*, 227(1-2), 13-30.

493 Dai, J., Liu, J.T., Wei, W., Chen, J., 2014. Detection of the Three Gorges Dam influence on
494 the Changjiang (Yangtze River) submerged delta. *Scientific reports*, 4: 6600.

495 Dou, G., Dong, F., Dou, X., Li, T., 1995. Mathematical modeling of sediment transport in
496 estuaries and coastal regions. *Science in China (Series A)*, 38(10), 1251-1260.

497 Fan, H., Huang, H., 2005. Changes in Huanghe (Yellow) River estuary since artificially re-
498 routing in 1996. *Chinese Journal of Oceanology and Limnology*, 23 (3), 299-305.

499 Fan, Y., Chen, S., Zhao, B., Pan, S., Jiang, C., Ji, H., 2018a. Shoreline dynamics of the active
500 Yellow River delta since the implementation of Water-Sediment Regulation Scheme: A
501 remote-sensing and statistics-based approach. *Estuarine, Coastal and Shelf Science*, 200,
502 406-419.

503 Fan, Y., Chen, S., Bo, Z., Yu, S., Ji, H., Jiang, C., 2018b. Monitoring tidal flat dynamics
504 affected by human activities along an eroded coast in the Yellow River Delta, China.
505 *Environmental Monitoring and Assessment*, 190, 396.

506 Hervouet, J.M., 2007. Hydrodynamics of free surface flows: modelling with the finite element
507 method. John Wiley & Sons.

508 Hoitink, A. J. F., Wang, Z. B., Vermeulen, B., Huismans, Y., Kästner, K., 2017. Tidal controls
509 on river delta morphology. *Nature geoscience*, 10(9), 637-645.

510 Huang, J, Xu, J., Gao, S., Lian, X., Li, J., 2015. Analysis of influence on the Bohai Sea tidal
511 system induced by coastline modification. *Journal of Coastal Research*, 73(sp1), 359-363.

512 Huzzey, L.M., Brubaker, J.M., 1998. The formation of longitudinal fronts in a coastal plain
513 estuary. *Journal of Geophysical Research*, 93 (C2), 1329–1334.

514 Ji, H., Chen, S., Pan, S., Xu, C., Jiang, C., Fan, Y., 2018. Morphological variability of the active
515 Yellow River mouth under the new regime of riverine delivery. *Journal of hydrology*, 564,
516 329-341.

517 Jiang, C., Pan, S., Chen, S., 2017. Recent morphological changes of the Yellow River
518 (Huanghe) submerged delta: Causes and environmental implications. *Geomorphology*,
519 293, 93-107.

520 Jiang, C., Chen, S., Pan, S., Fan, Y., Ji, H., 2018. Geomorphic evolution of the Yellow River
521 Delta: Quantification of basin-scale natural and anthropogenic impacts. *Catena*, 163, 361-
522 377.

523 Li, G., Wei, H., Yue, S., Cheng, Y., Han, Y., 1998. Sedimentation in the Yellow River delta,
524 part II: suspended sediment dispersal and deposition on the subaqueous delta. *Marine*
525 *Geology*, 149(1), 113-131.

526 Li, G., Tang, Z., Yue, S., Zhuang, K., Wei, H., 2001. Sedimentation in the shear front off the
527 Yellow River mouth. *Continental Shelf Research*, 21, 607-625.

528 Leonardi, N., Canestrelli, A., Sun, T., Fagherazzi, S., 2013. Effect of tides on mouth bar
529 morphology and hydrodynamics, *Journal of Geophysical Research: Oceans*, 118, 1-15.

530 Leonardi, N., Kolker, A. S., Fagherazzi, S., 2015. Interplay between river discharge and tides
531 in a delta distributary. *Advances in water resources*, 80, 69-78.

532 Li, Y.F., Zhang, H., Tang, C., Zou, T., Jiang, D.L., 2016. Influence of Rising Sea Level on
533 Tidal Dynamics in the Bohai Sea. *Journal of Coastal Research*, 74(sp1), 22-31.

534 Liu, F., Chen, S., Dong, P., Peng, J., 2012. Spatial and temporal variability of water discharge
535 in the Yellow River Basin over the past 60 years. *Journal of Geographical Sciences*, 22(6),
536 1013-1033.

537 Luan, H.L., Ding, P.X., Wang, Z.B., Ge, J.Z., Yang, S.L., 2016. Decadal morphological
538 evolution of the Yangtze Estuary in response to the river input changes and estuarine
539 engineering projects. *Geomorphology*, 265, 12-23.

540 Maloney, J.M., Bentley S.J., Xu, K., Obelcz, J., Georgiou, I.Y., Miner, M.D., 2018. Mississippi
541 River subaqueous delta is entering a stage of retrogradation. *Marine Geology*, 400, 12-23.

542 Milliman, J.D., Meade, R.H., 1983. World-wide delivery of river sediment to the oceans. *The*
543 *Journal of Geology*, 91(1), 1-21.

544 Nienhuis, J. H., Hoitink, A. J. F., Törnqvist, T. E., 2018. Future Change to Tide- Influenced
545 Deltas. *Geophysical Research Letters*, 45(8), 3499-3507.

546 Nunes, R.A., Simpson, J.H., 1985. Axial convergence in a well-mixed estuary. *Estuarine,*
547 *Coastal and Shelf Science*, 20, 637–649.

548 Pawlowicz, R., Beardsley, B., Lentz, S., 2002. Classical tidal harmonic analysis including error
549 estimates in MATLAB using T_TIDE. *Computers & Geosciences*, 28(8), 929-937.

550 Peng, J., Chen, S., Dong, P., 2010. Temporal variation of sediment load in the Yellow River
551 basin, China, and its impacts on the lower reaches and the river delta. *Catena*, 83, 135-147.

552 Pelling, H.E., Uehara, K., Green, J.A.M., 2013. The impact of rapid coastline changes and sea
553 level rise on the tides in the Bohai Sea, China. *Journal of Geophysical Research: Oceans*,
554 118, 3462-3472.

555 Qiao, L.L., Bao, X.W., Wu, D.X., Wang, X.H., 2008. Numerical study of generation of the
556 tidal shear front off the Yellow River mouth. *Continental Shelf Research*. 28 (14), 1782–
557 1790.

558 Qiu, Z., Xiao, C., Perrie, W., Sun, D., Wang, S., Shen, H., Yang, D., He, Y., 2017. Using
559 Landsat 8 data to estimate suspended particulate matter in the Yellow River estuary.
560 Journal of Geophysical Research: Oceans, 122, 276-290.

561 Reeve, D., Chadwick, A., Fleming, C., 2004. Coastal Engineering: processes, theory and design
562 practice. Spon Press, London; New York

563 Syvitski, J.P.M., Saito, Y., 2007. Morphodynamics of deltas under the influence of humans.
564 Global and Planetary Change, 57(3-4), 261-282.

565 Wang, H., Yang, Z., Saito, Y., Liu, J.P., Sun, X., 2006a. Interannual and seasonal variation of
566 the Huanghe (Yellow River) water discharge over the past 50 years: Connections to
567 impacts from ENSO events and dams. Global and Planetary Change, 50(3-4), 212-225.

568 Wang, H., Yang, Z., Bi, N., 2006b. 3-D simulation of the suspended sediment transport in the
569 Yellow River mouth, shear front off the Yellow River mouth. Journal of Sediment
570 Research. 2, 1–9. (In Chinese with English abstract).

571 Wang, H., Yang, Z., Li, Y., Guo, Z., Sun, X., Wang, Y., 2007. Dispersion pattern of suspended
572 sediment in the shear frontal zone off the Huanghe (Yellow River) mouth. Continental
573 Shelf Research, 27 (6), 854–871.

574 Wang, H., Bi, N., Wang, Y., Saito, Y., Yang, Z., 2010. Tide-modulated hyperpycnal flows off
575 the Huanghe (Yellow River) mouth, China. Earth Surface Processes and Landforms,
576 35(11), 1315-1329.

577 Wang, N., Li, G., Qiao, L., Shi, J., Dong, P., Xu, J., Ma, Y., 2017a. Long-term evolution in the
578 location, propagation, and magnitude of the tidal shear front off the Yellow River Mouth.
579 Continental Shelf Research, 137, 1-12.

580 Wang, Y., Liu, D., Lee, K., Dong, Z., Di, B., Wang, Y., Zhang, J., 2017b. Impact of Water-
581 Sediment Regulation Scheme on seasonal and spatial variations of biogeochemical factors
582 in the Yellow River estuary. *Estuarine, Coastal and Shelf Science*, 198, 92-105.

583 Wiseman, W. J., Fan, Y.-B., Bornhold, B.D., Keller, G.H., Su, Z.-Q., Prior, D.B., Yu, Z.-X.,
584 Wright, L.D., Wang, F.-Q, Qian, Q.-Y., 1986. Suspended sediment advection by tidal
585 currents off the Huanghe (Yellow River) delta. *Geo-Marine Letters*, 6(2), 107-113.

586 Wright, L.D., Wiseman, W.J., Bornhold, B.D., Prior, D.B., Suhayda, J.N., Keller, G.H., Yang,
587 Z.-S., Fan, Y.B., 1988. Marine dispersal and deposition of Yellow River silts by gravity-
588 driven underflows. *Nature*, 332(6165), 629-632.

589 Wright, L.D., Wiseman, W.J., Yang, Z.S., Bornhold, B.D., Keller, G.H., Prior, D.B., Suhayda,
590 J.N., 1990. Processes of marine dispersal and deposition of suspended silts off the modern
591 mouth of the Huanghe (Yellow River). *Continental Shelf Research*, 10(1), 1-40.

592 Wright, L.D., Yang, Z.S., Bornhold, B.D., Keller, G.H., Prior, D.B., Wiseman, W.J., 1986.
593 Hyperpycnal plumes and plume fronts over the Huanghe (Yellow River) delta front. *Geo-*
594 *Marine Letters*, 6(2), 97-105.

595 Wu, X., Bi, N., Yuan, P., Li, S., Wang, H., 2015. Sediment dispersal and accumulation off the
596 present Huanghe (Yellow River) delta as impacted by the water-Sediment Regulation
597 Scheme. *Continental shelf Research*, 111, 236-138.

598 Yang, Z., Ji, Y., Bi, N., Lei, K., Wang, H., 2011. Sediment transport off the Huanghe (Yellow
599 River) delta and the adjacent Bohai Sea in winter and seasonal comparison. *Estuarine,*
600 *Coastal and Shelf Science*, 93, 173-181.

Yu, Y., Wang, H., Shi, X., Ran, X., Cui, T., Qiao, S., Liu, Y., 2013. New discharge regime of the Huanghe (Yellow River): Causes and implications. *Continental Shelf Research*, 69, 62-72.

Zhou, Y., Huang, H.Q., Nanson, G.C., Huang, C., Liu, G., 2015. Progradation of the Yellow (Huanghe) River delta in response to the implementation of a basin-scale water regulation program. *Geomorphology*, 243: 65-74.

Zhu, L., Hu, R., Zhu, H., Jiang, S., Xu, Y., Wang, N., 2018. Modeling studies of tidal dynamics and the associated responses to coastline changes in the Bohai Sea, China. *Ocean Dynamics*, 68, 1625-1648.

Figure captions

Figure 1. (a) Map of the Yellow River basin, where dots indicate the major hydrological stations including Tangnaihai (TNH), Lanzhou (LZ), Toudaoguai (TDG), Longmen (LM), Huayuankou (HYK), Lijin (LJ); and triangles represent large hydraulic engineering projects (dams and reservoirs) in the basin; (b) Map of the modern Yellow River Delta, with a geographic view of the lowermost channel shifts, river mouth, and subaqueous morphology.

Figure 2. Monthly distribution of (a) water discharge Q ; (b) sediment load Q_s ; (c) SSC; (d) median grain size from 1962 to 2017.

Figure 3. Computational domain and locations of tide gauges (squares) and velocity observations (triangles).

Figure 4. The comparisons of the computed and measured water levels.

Figure 5. Comparisons of the computed and measured flow velocities and directions.

Figure 6. Comparison with the computed SSC and a remote sensing image.

623 Figure 7. Co-tidal charts for: (a) O1, (b) K1, (c) M2 and (d) S2 tide constituents, (e)
624 distributions of tidal ranges, and (f) tidal ratio.

625 Figure 8. Tidal amplitude differences for: (a-d) M2 and (e-h) K1 with water discharges of 500
626 m^3/s , 1000 m^3/s , 4000 m^3/s and 10000 m^3/s respectively against the reference case (0 m^3/s).

627 Figure 9. Computed water levels at P0 (the location as shown in [Figure 8h](#)) of the tidal flat at
628 the active YRD with prescribed river flow discharges.

629 Figure 10. Velocity distributions near the shear front zone: (a) IFOE type and (b) IEOF type.

630 Figure 11. The formation and propagation of the shear front of: (a) IFOE; (b) IEOF

631 Figure 12. Flow direction variations at P1 and P2, where the grey rectangles indicate the
632 durations of both types of shear front.

633 Figure 13. Locations of the shear front zone (velocity less than 0.10 m/s) with river discharges
634 of 500 m^3/s , 2000 m^3/s and 3000 m^3/s for types (a) IFOE and (b) IEOF.

635 Figure 14. Velocity distributions under different river discharges: (a) IFOE along S1, (b) IEOF
636 along S1, (c) IFOE along S2, and (d) IEOF along S2. Velocities are section-perpendicular (+ve
637 = Northward and -ve = Southward) and the reversal locations of the flow are marked with
638 circles).

639 Figure 15. SSC distributions with: (a) IFOE and (b) IEOF along profiles S1; (c) IFOE and (d)
640 IEOF along profile S2, where the circles indicate the reversal locations of flow under different
641 river discharges.

642 Figure 16. Suspended sediment transport rate (Q_s) at: (a) maximum flood, (b) maximum ebb
643 phases, and depo-centers with river discharges of: (c) 500 m^3/s and (d) 3000 m^3/s .

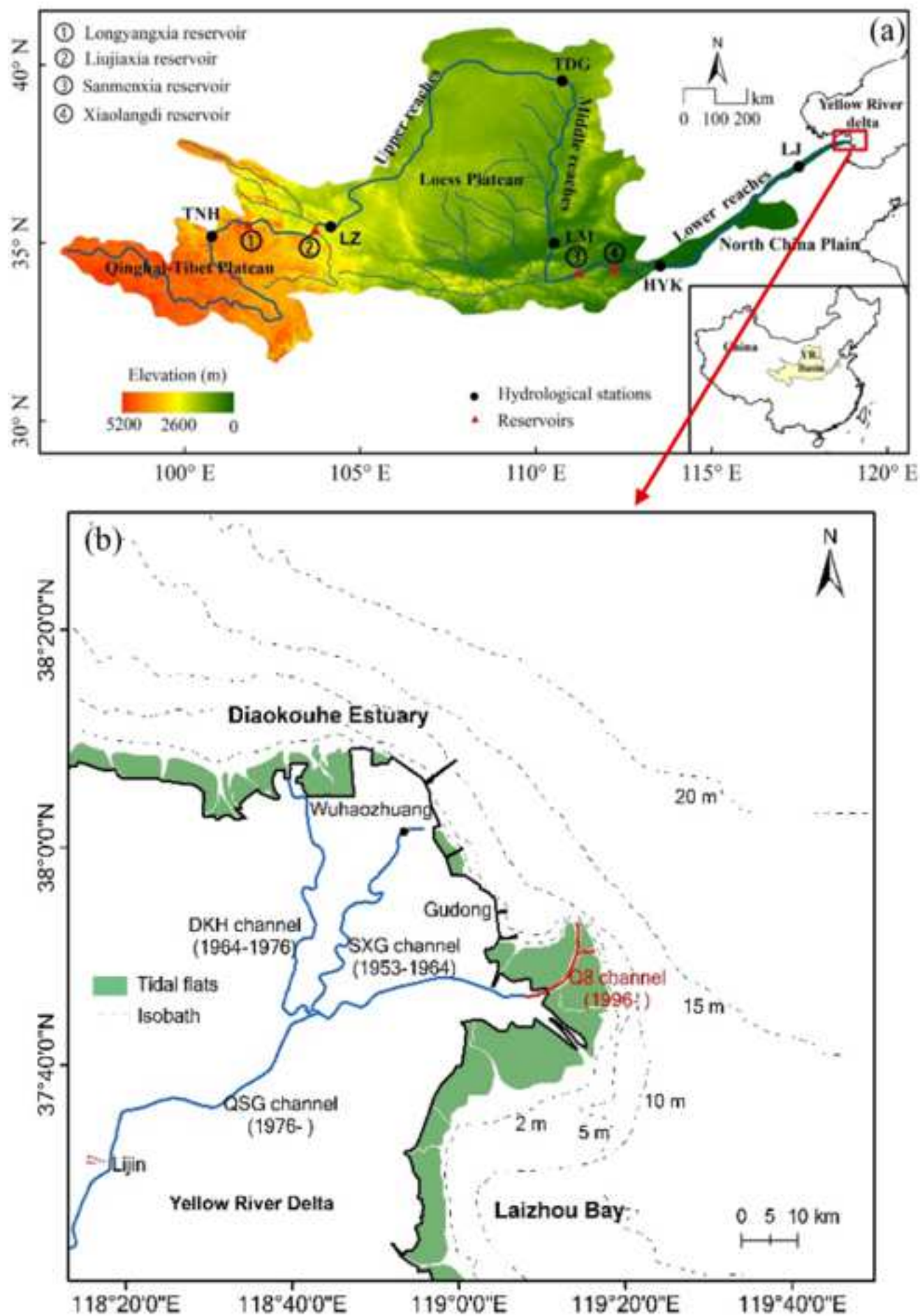


Figure 2

[Click here to download Figure Figure2.tif](#)

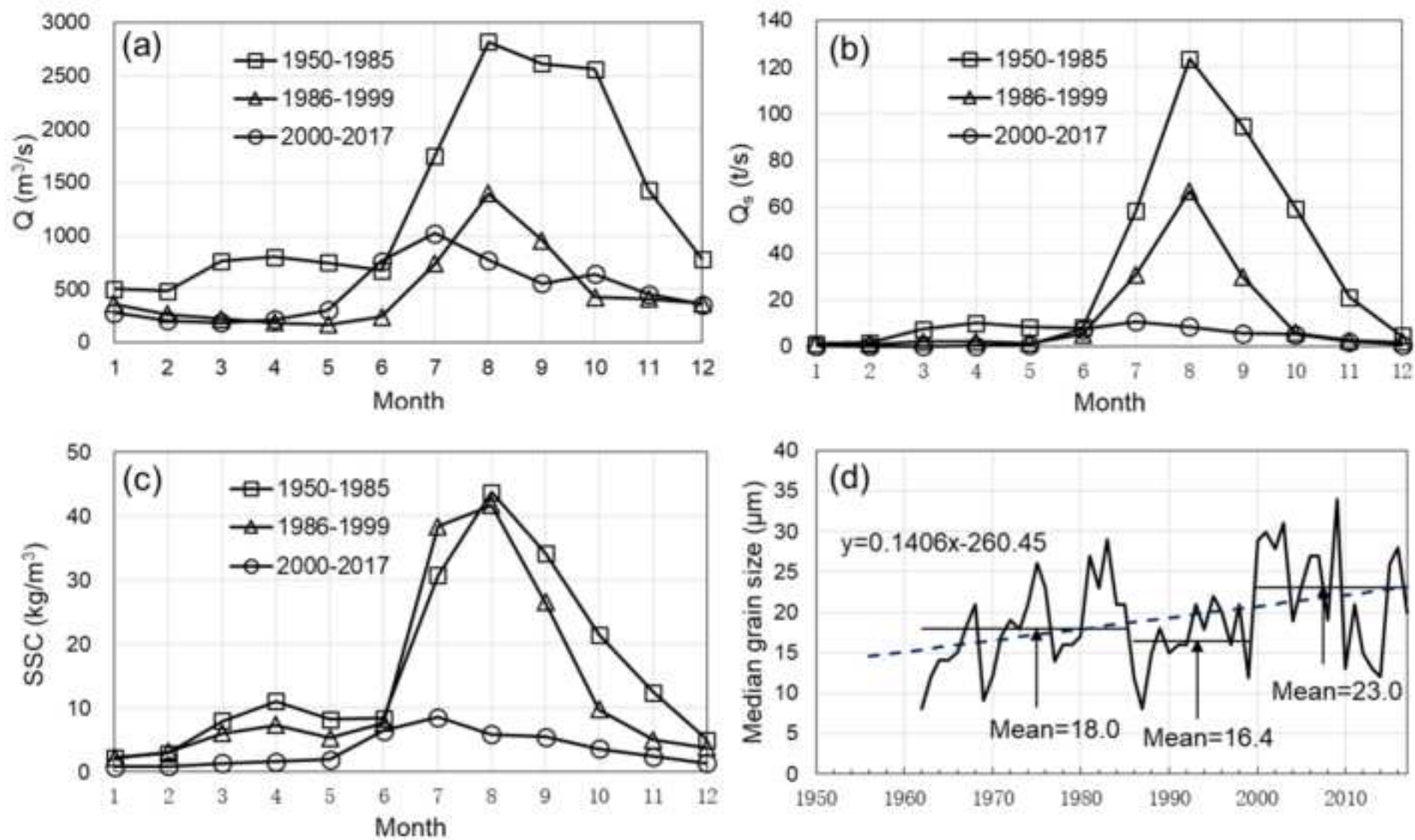
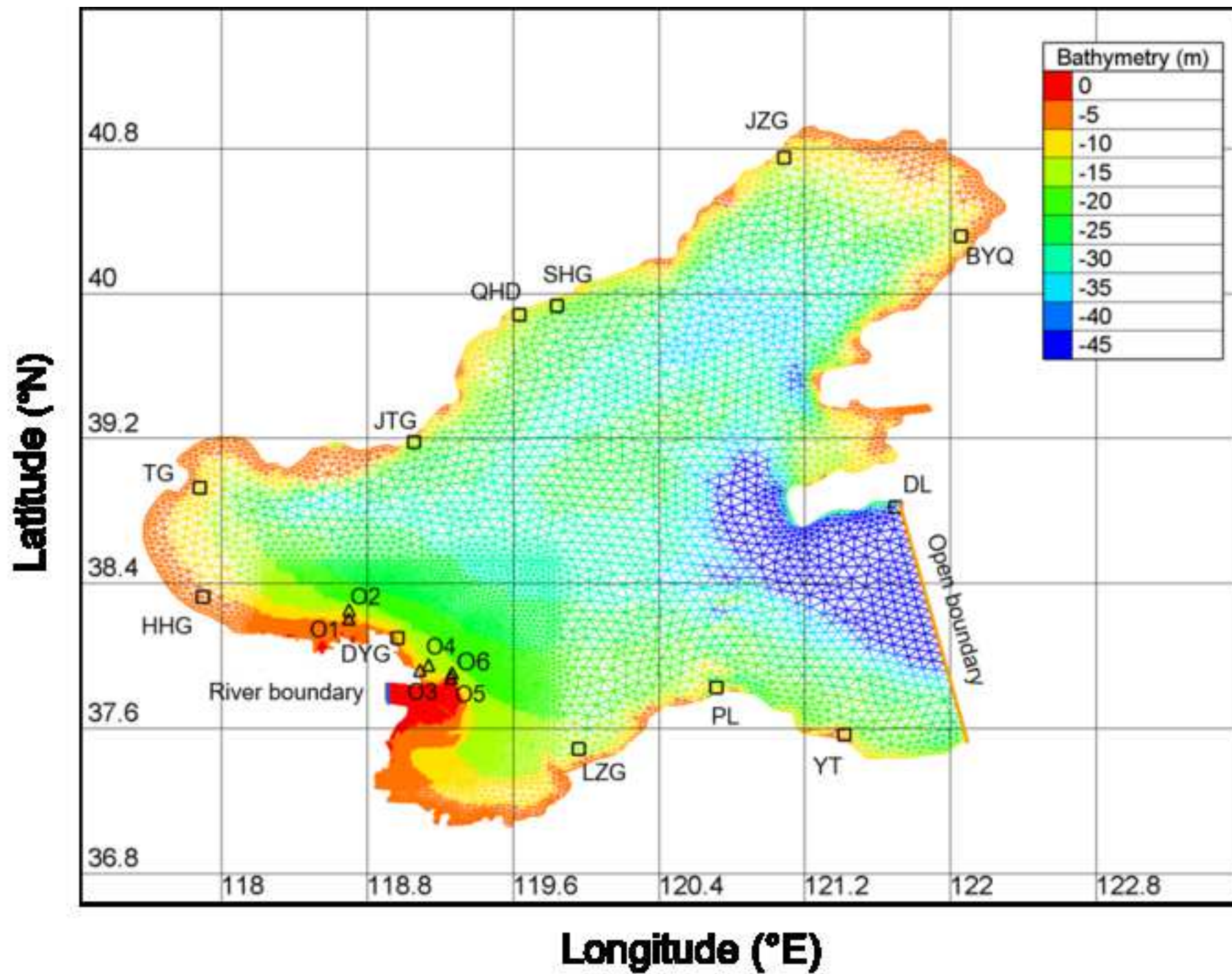


Figure 3

[Click here to download Figure Figure3.tif](#)



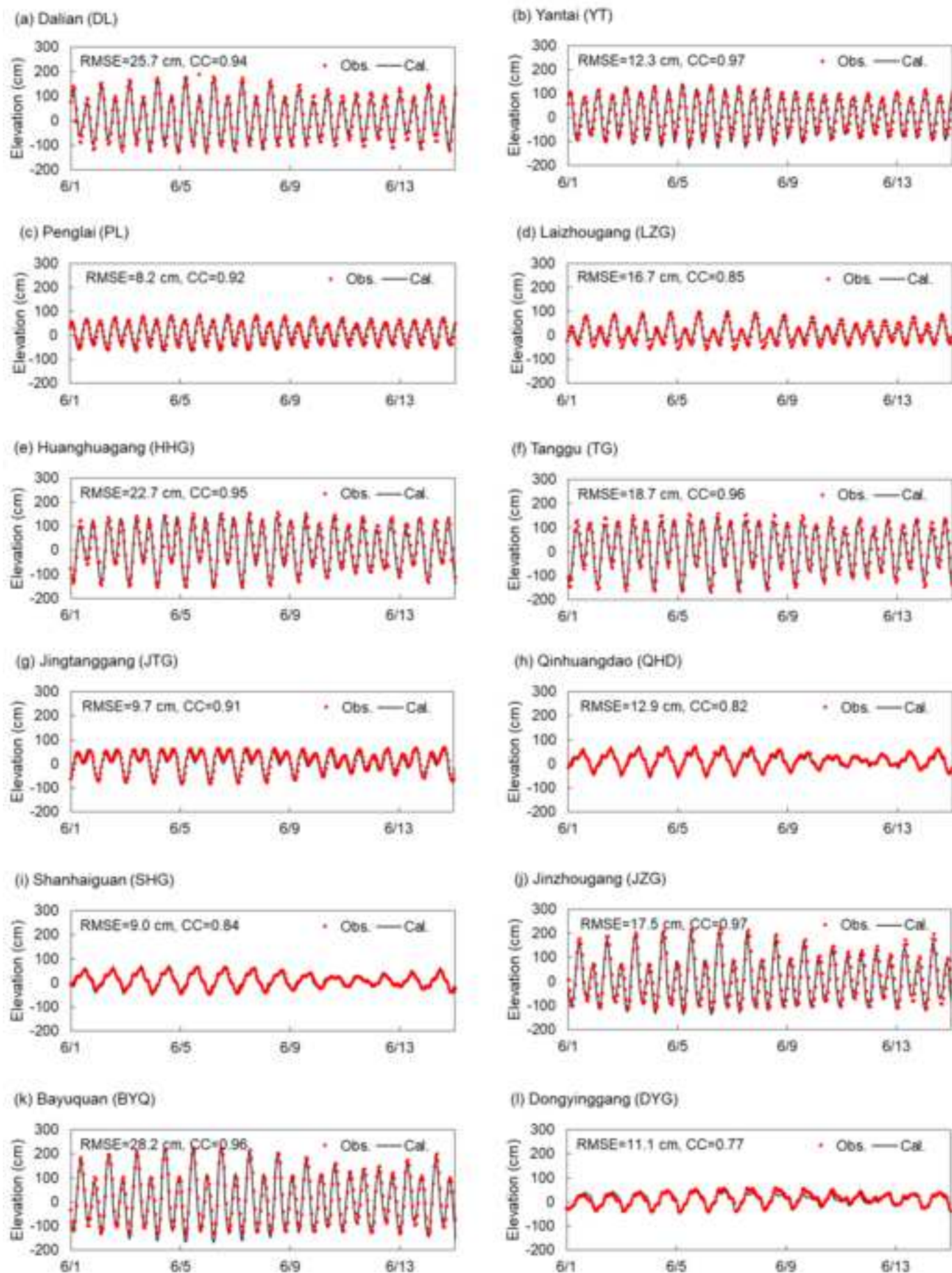


Figure 5

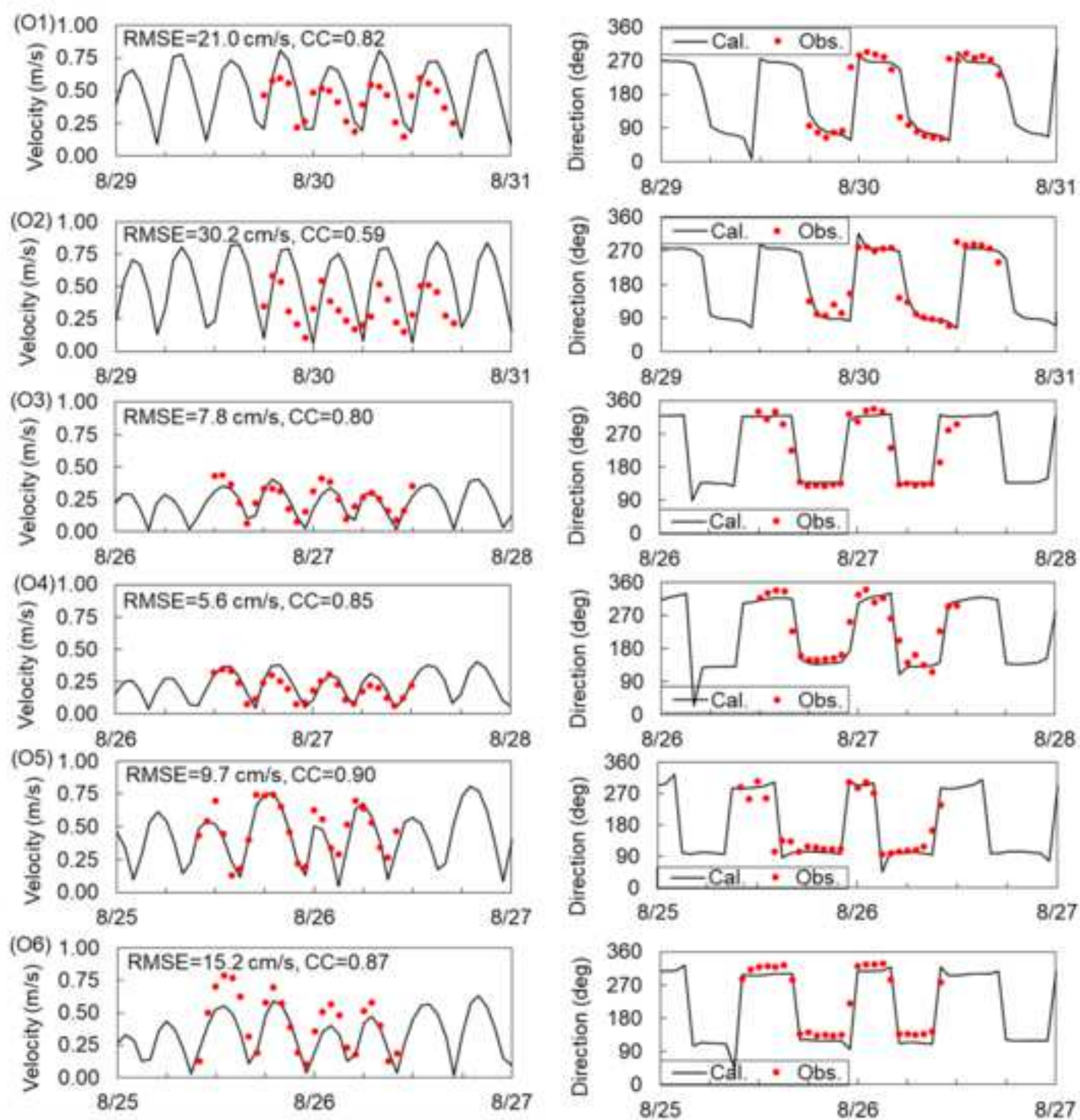
[Click here to download Figure Figure5.tif](#)

Figure 6

[Click here to download Figure Figure6.tif](#)

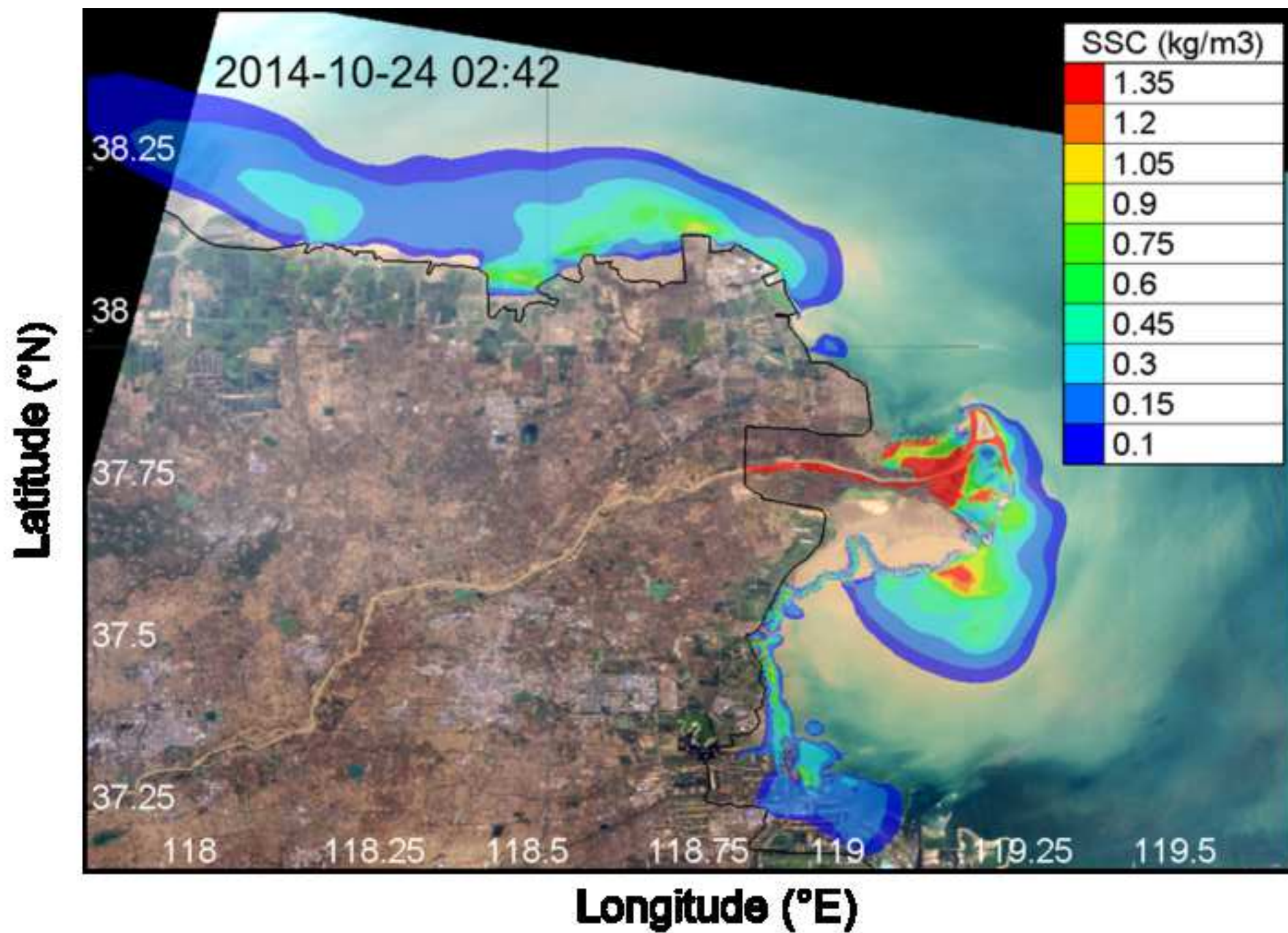


Figure 7

[Click here to download Figure Figure7.tif](#)

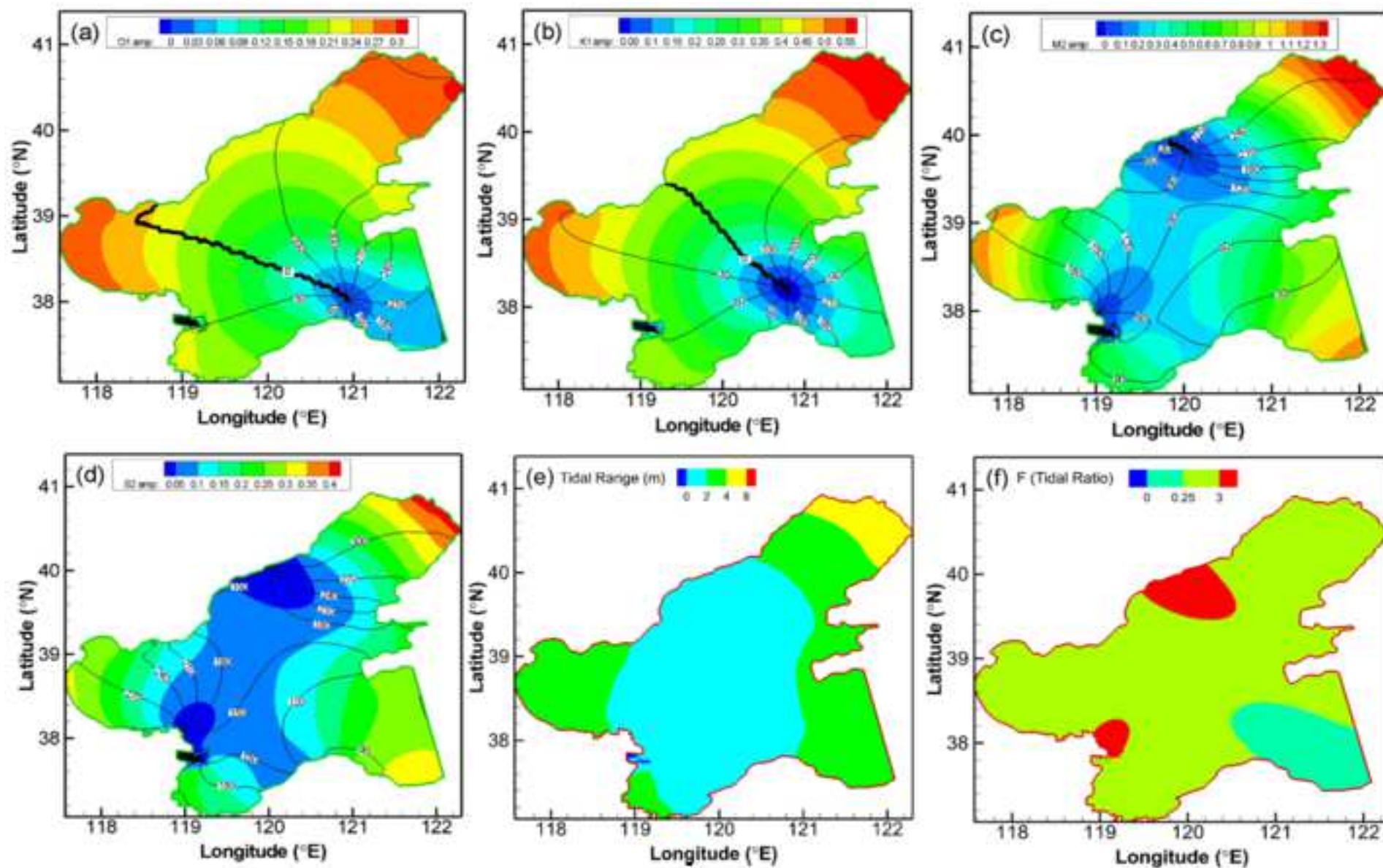


Figure 8

[Click here to download Figure8.tif](#)

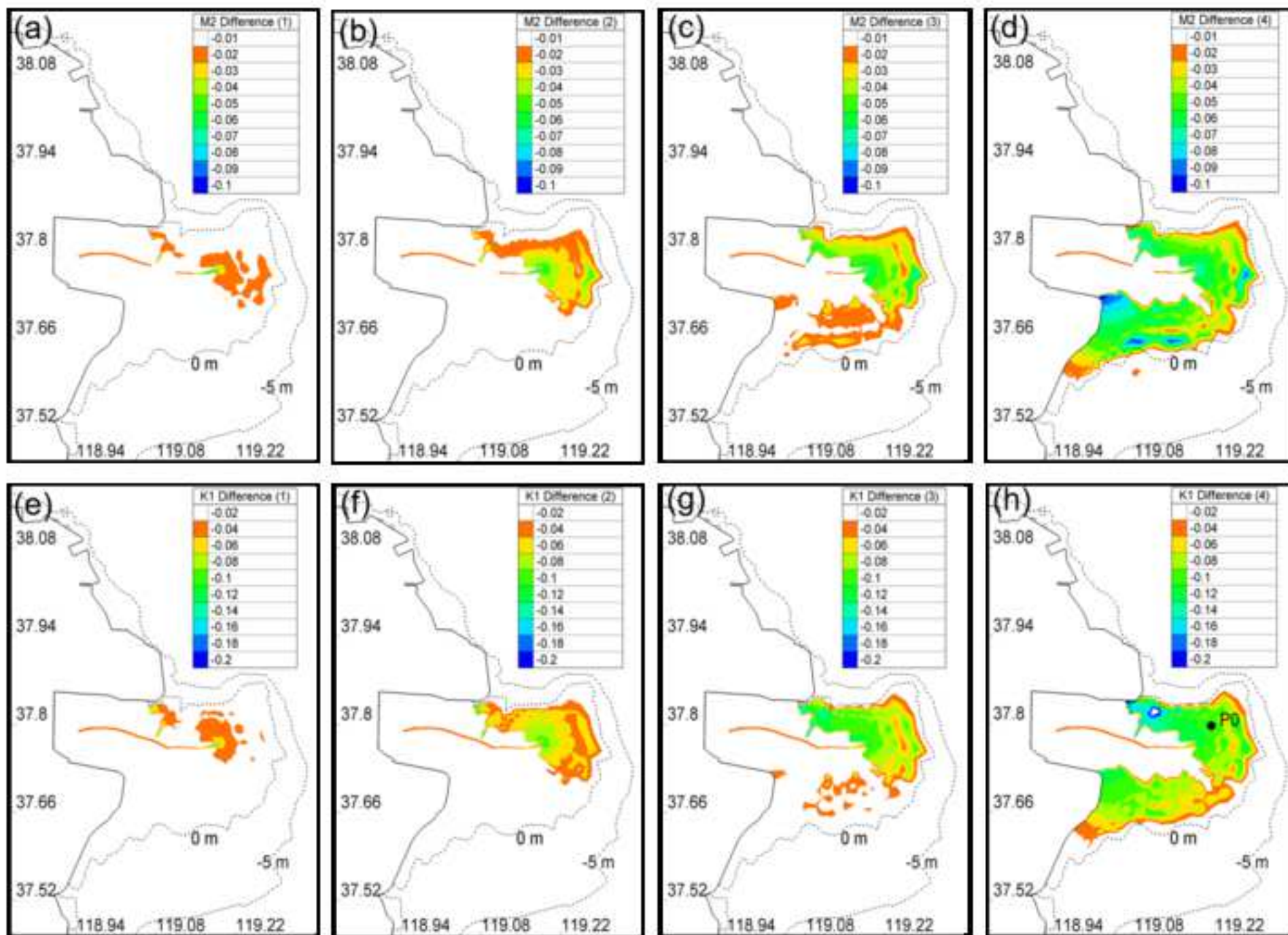
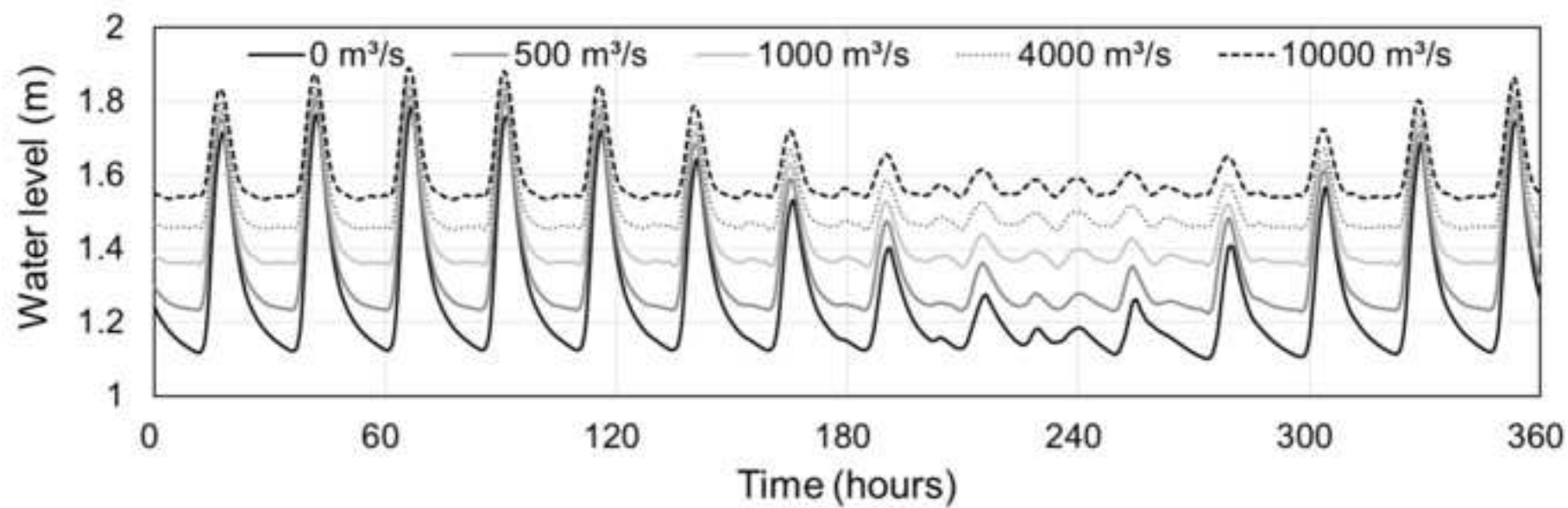
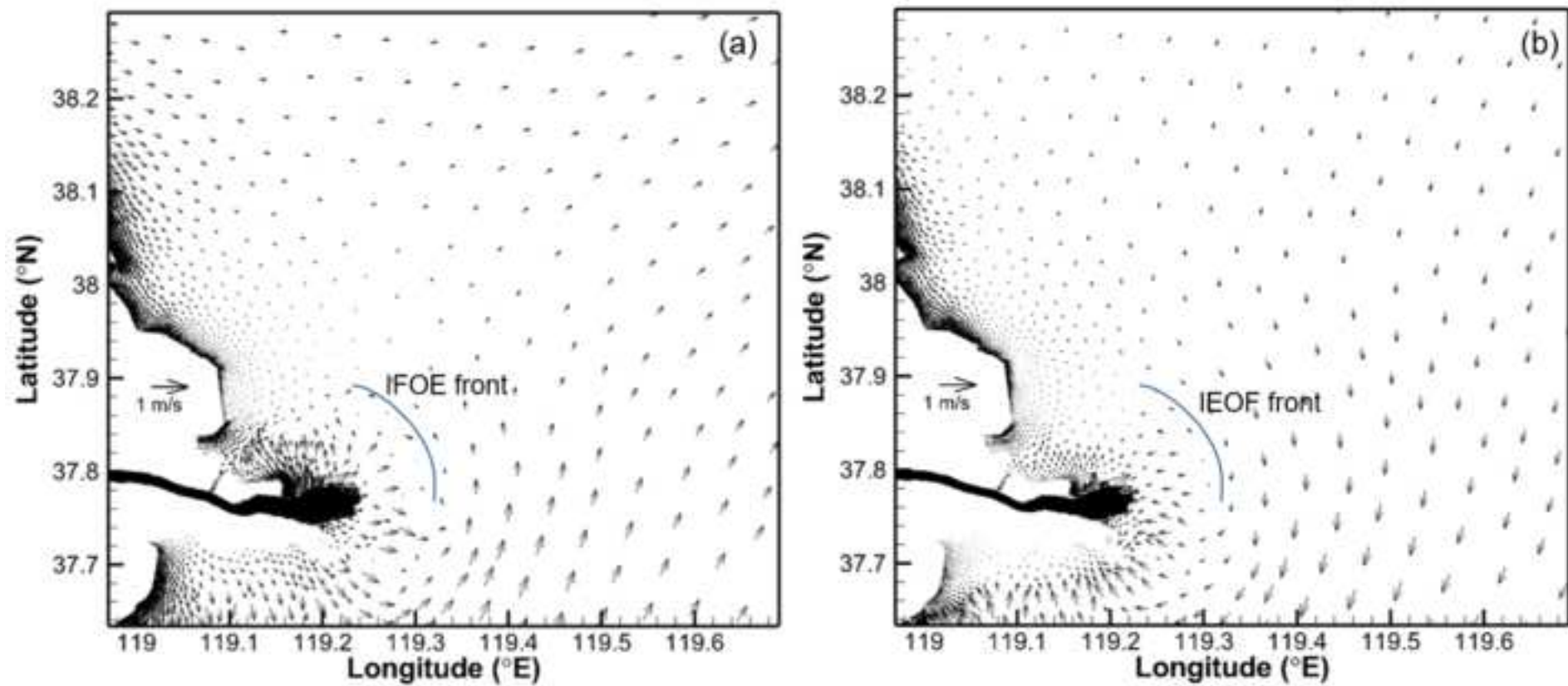
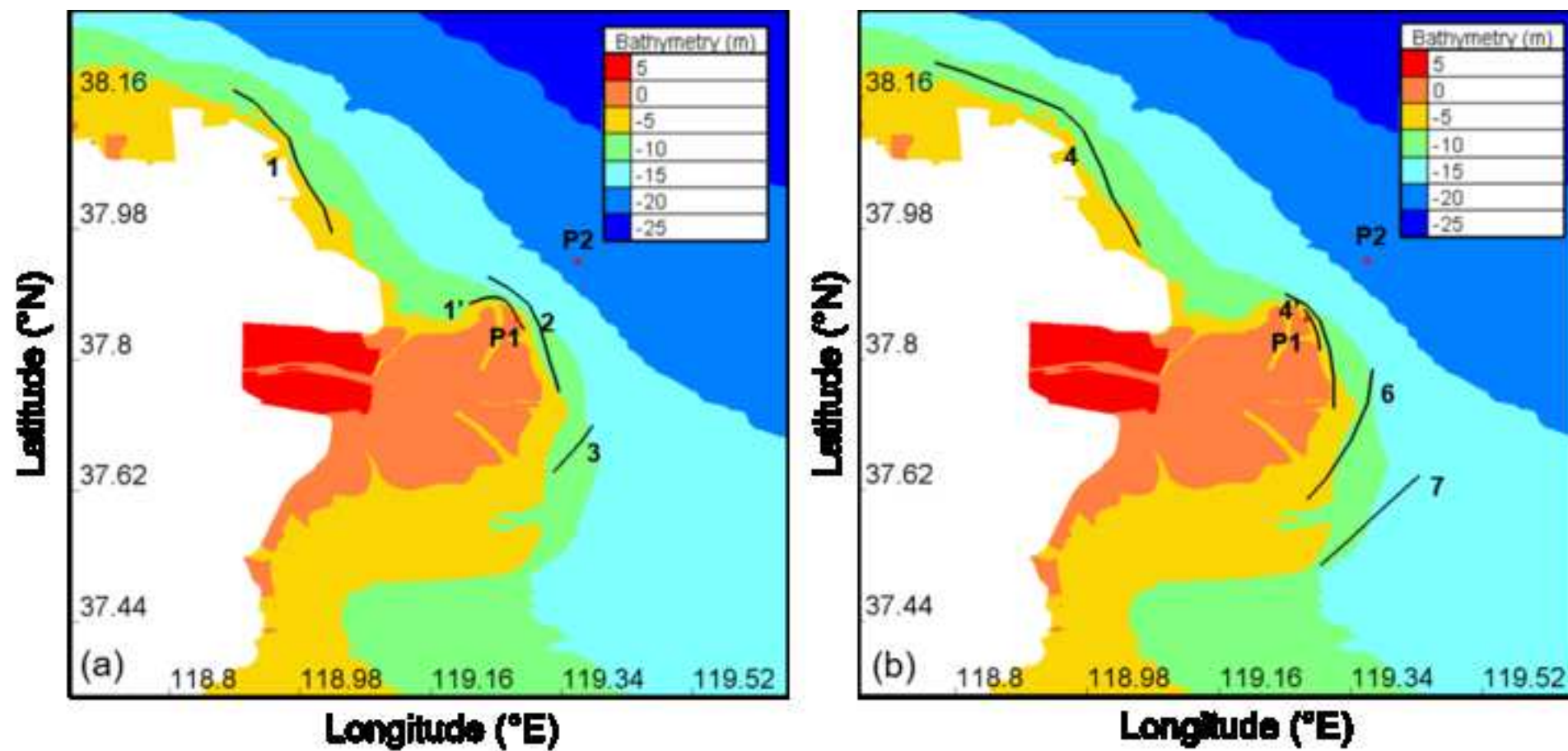
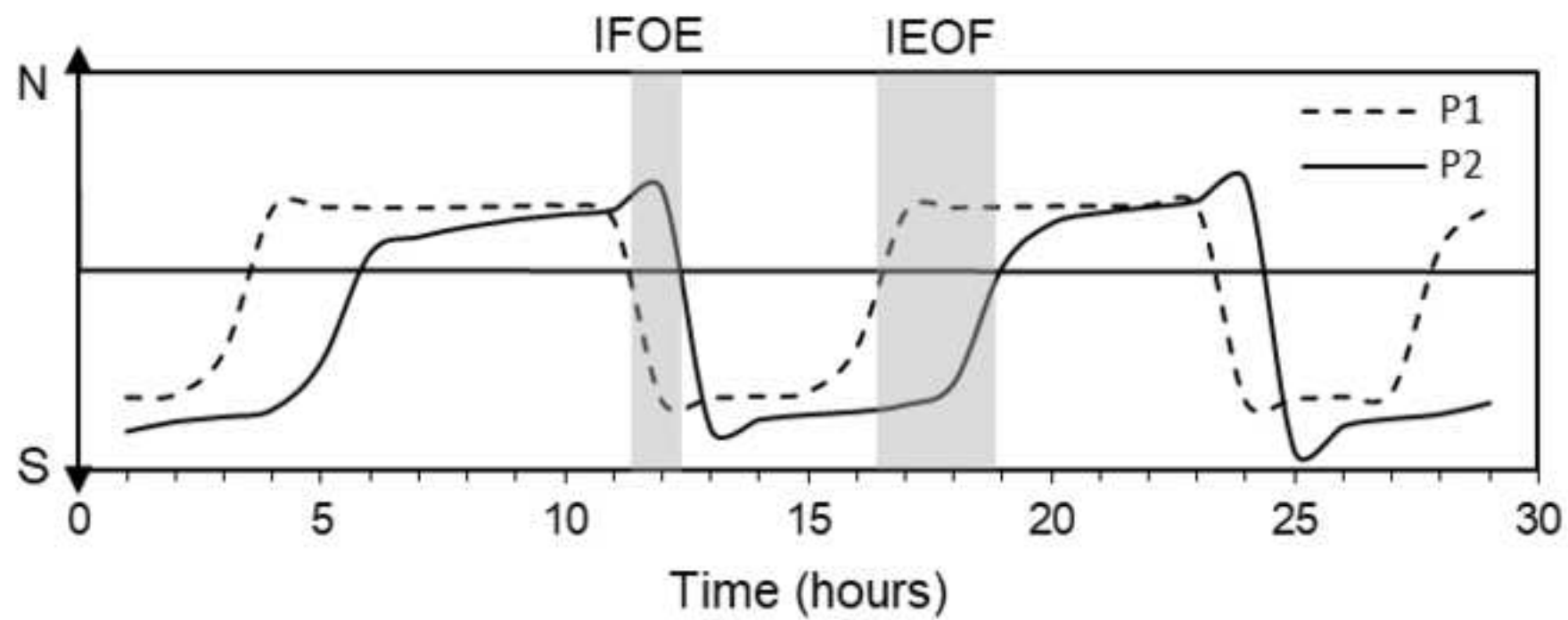


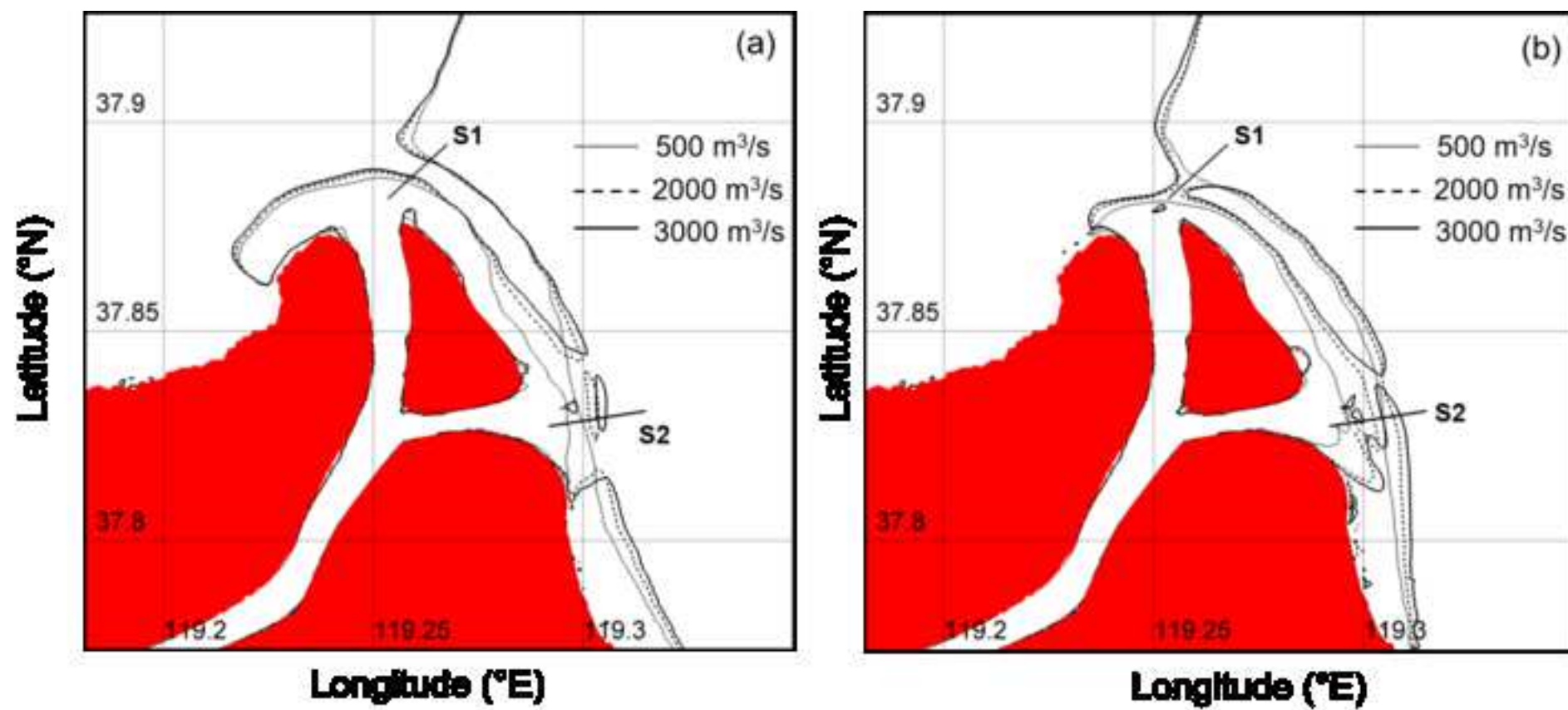
Figure 9

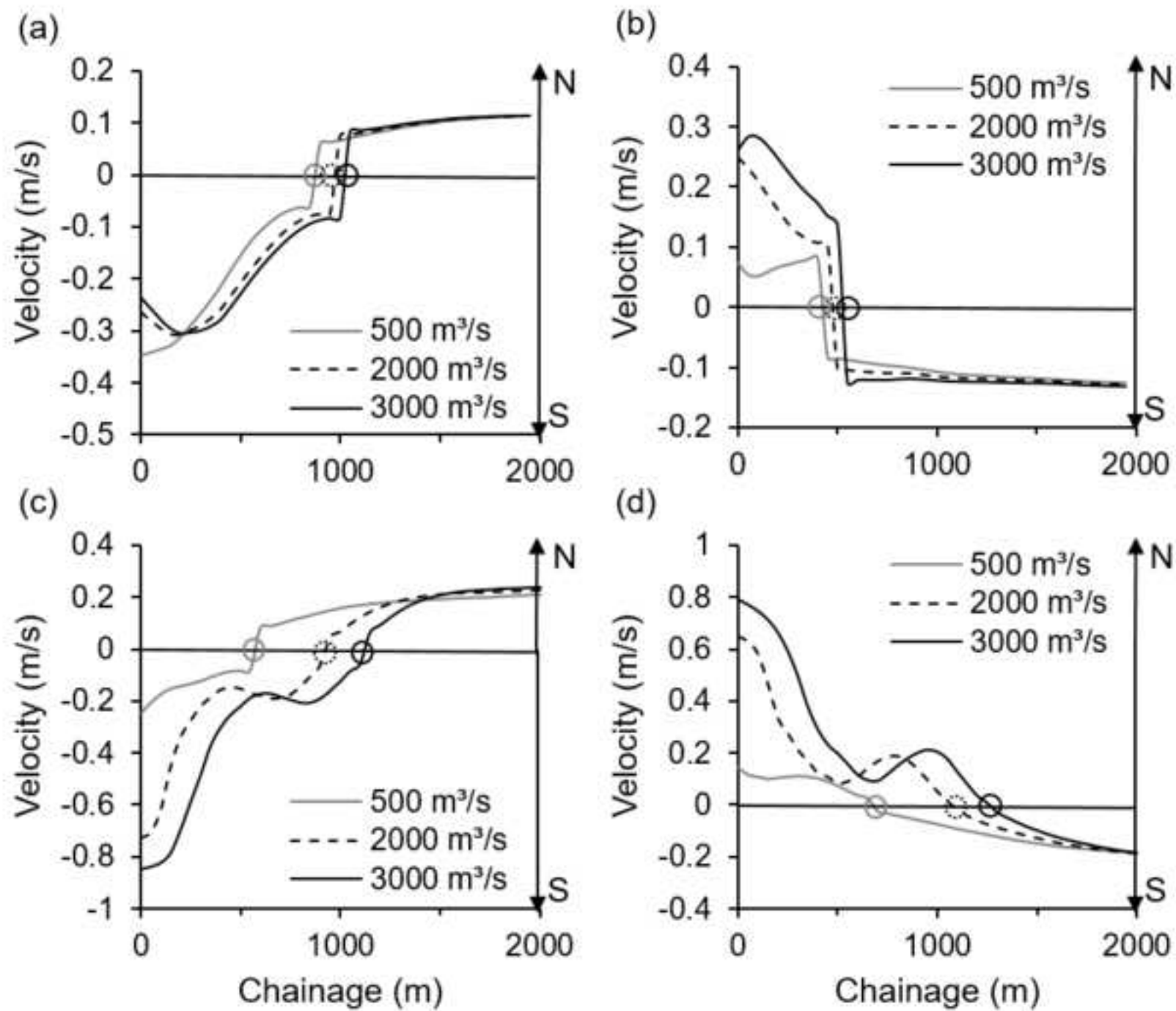


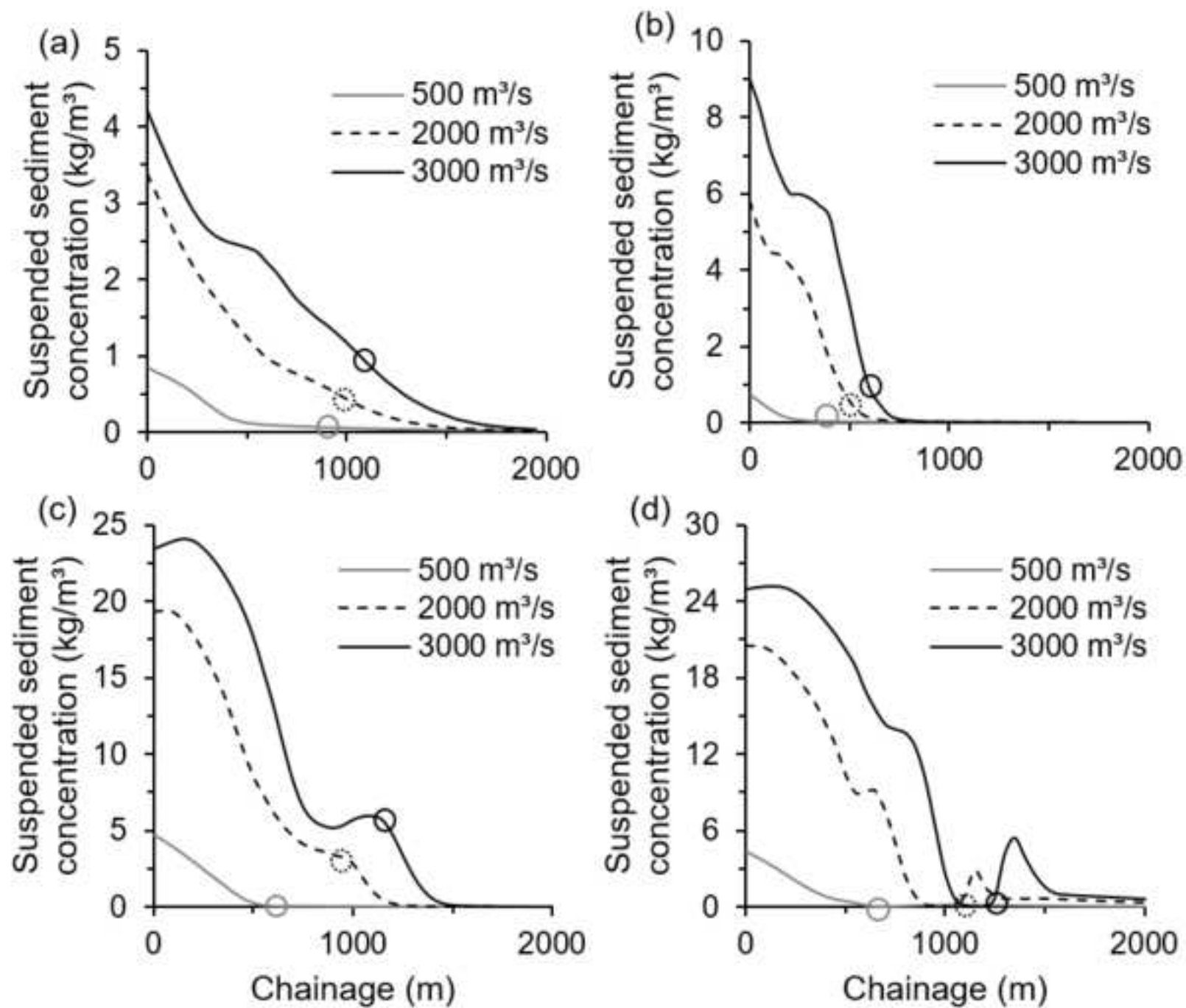


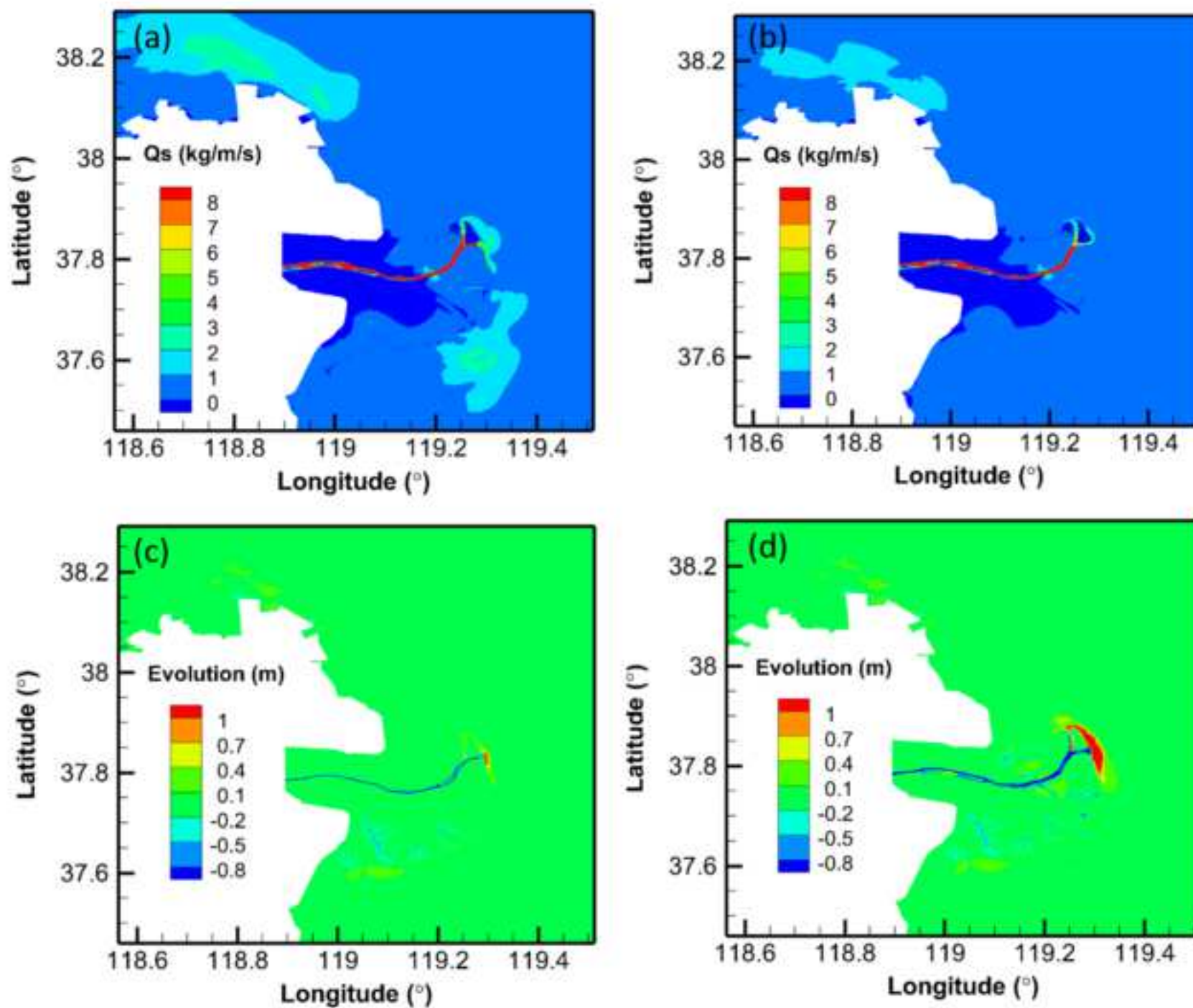












Declaration of interests

☒ The authors declare that they have no known competing financial interests or personal relationships that could have appeared to influence the work reported in this paper.

☐The authors declare the following financial interests/personal relationships which may be considered as potential competing interests: